Int J Earth Sci (Geol Rundsch) (2011) 100:1029–1063
DOI 10.1007/s00531-010-0622-2

ORIGINAL PAPER

3-D assessment of peak-metamorphic conditions by Raman spectroscopy of carbonaceous material: an example from the margin of the Lepontine dome (Swiss Central Alps)

Michael Wiederkehr · Romain Bousquet · Martin A. Ziemann · Alfons Berger · Stefan M. Schmid

Received: 30 March 2010 / Accepted: 7 November 2010 / Published online: 21 January 2011

Abstract This study monitors regional changes in the crystallinity of carbonaceous matter (CM) by applying Micro-Raman spectroscopy to a total of 214 metasediment samples (largely so-called Bündnerschiefer) dominantly metamorphosed under blueschist- to amphibolite-facies conditions. They were collected within the northeastern margin of the Lepontine dome and easterly adjacent areas of the Swiss Central Alps. Three-dimensional mapping of isotemperature contours in map and profile views shows that the isotemperature contours associated with the Miocene Barrow-type Lepontine metamorphic event cut across refolded nappe contacts, both along and across strike within the northeastern margin of the Lepontine dome and adjacent areas. Further to the northeast, the isotemperature contours reflect temperatures reached during the Late Eocene subduction-related blueschist-facies event and/or during subsequent near-isothermal decompression; these contours appear folded by younger, large-scale post-nappe-stacking folds. A substantial jump in the recorded maximum temperatures across the tectonic contact between the frontal Adula nappe complex and surrounding metasediments indicates that this contact accommodated differential tectonic movement of the Adula nappe with respect to the enveloping Bündnerschiefer after maximum temperatures were reached within the northern Adula nappe, i.e. after Late Eocene time.

Keywords HP-metamorphism · Barrovian metamorphism · Graphitization · Metasediments · Micro-Raman spectroscopy · Central Alps

M. Wiederkehr (✉) · S. M. Schmid
Geologisch-Paläontologisches Institut, Universität Basel, Bernoullistrasse 32, 4056 Basel, Switzerland
e-mail: michael.wiederkehr@gmx.ch

M. Wiederkehr · R. Bousquet · M. A. Ziemann
Institut für Erd- und Umweltwissenschaften, Universität Potsdam, Karl-Liebknecht-Strasse 24/25, 14476 Potsdam/Golm, Germany

A. Berger
Institut for Geografi og Geologi, Københavns Universitet, Øster Voldgade 10, 1350 København K, Denmark

Present Address:
S. M. Schmid
Institut für Geologische Wissenschaften, Freie Universität Berlin, Malteserstrasse 74-100, 12249 Berlin, Germany

Present Address:
M. Wiederkehr
Geotechnisches Institut AG, Hochstrasse 48, 4002 Basel, Switzerland

Introduction

The metamorphic structure of the Alps reflects long-lasting plate convergence and collision between the European and Adriatic continental plates in Cretaceous to Cenozoic times (e.g. Trümpy 1960; Frisch 1979; Tricart 1984; Schmid et al. 1996; Handy et al. 2010). The geodynamic evolution and resulting metamorphic zonation of the Central Alps (Lepontine) and easterly adjacent areas are related to Cenozoic orogeny (e.g. Schmid et al. 1996; Bousquet et al. 2008) that followed an earlier Cretaceous cycle (Froitzheim et al. 1994; Schmid et al. 2008) only preserved in the Austroalpine units (e.g. Handy and Oberhänsli 2004; and references therein) and is therefore not addressed in this study. The metamorphic evolution can be subdivided into two distinct stages: (1) Latest Cretaceous—Late Eocene subduction-related pressure-dominated metamorphism and deformation (see review in Berger and Bousquet

2008; and references therein) that affected oceanic lithosphere formed during the opening of the Alpine Tethys as well as small parts of the immediately adjacent Europe-derived continental lithosphere; and (2) Oligocene—Middle Miocene temperature-dominated, Barrow-type metamorphism (Köppel et al. 1981; Hunziker et al. 1992; Berger et al. 2009; Janots et al. 2009; Rubatto et al. 2009) related to the collision between Europe and Adria. Collision involved accretion of massive volumes of crustal material derived from the lower, European plate (e.g. Lepontine dome and Tauern window; Bousquet et al. 1997; Schmid et al. 2004; Wiederkehr et al. 2008) to the upper plate comprising the older Austroalpine nappes and their previously accreted high-pressure units (e.g. Handy et al. 2010).

Several pioneering studies on the spatial distribution of index minerals as well as on different metamorphic facies types established the zonation of Alpine metamorphism, particularly within the Lepontine dome of the Central Alps (e.g. Wenk 1962, 1970; Niggli and Niggli 1965; Trommsdorff 1966; Frey 1969, 1978; Niggli 1970; Frey et al. 1980, 1999; Oberhänsli et al. 2004). However, the metamorphic zonation related to pressure-dominated metamorphism should be distinguished from that related to Barrovian overprint in the Alps. Whereas the pressure-dominated units (blueschists and eclogites) form a continuous belt striking parallel to the orogenic trend, remnants of the temperature-dominated event are localized, primarily in the Lepontine dome and the Tauern window (e.g. Goffé et al. 2003; Bousquet et al. 2008). From a geodynamic point of view, only the Central Alps (Lepontine dome) and the Tauern window in the Eastern Alps reached the mature stage of a collisional orogenic belt characterized by pervasive Barrovian overprint. The Western Alps never reached this stage and hence can be interpreted as a frozen-in subduction zone (Bousquet 2008).

This study addresses a key area for the reconstruction of the Alpine geodynamic evolution at the northeastern margin of the Lepontine dome and adjacent areas further east in which both pressure- and temperature-dominated metamorphic domains are found to be in close contact. This provides important constraints on the metamorphic evolution of the Central Alps during the transition from subduction to collision (e.g. Bousquet et al. 2002; Wiederkehr et al. 2008, 2009). The metasediments studied, predominantly calcschists, have great potential for recording the metamorphic evolution and can therefore be used for the geodynamic reconstruction of the Alpine orogenic belt (see also Goffé and Chopin 1986; Wiederkehr et al. 2008, 2009). Moreover, these metasediments cover large areas, making them ideal for correlating the structural and metamorphic evolution over long distances. This is rarely possible in mafic rocks, which usually occur only as dismembered and isolated bodies.

Despite the remarkable progress made on reconstructing the metamorphic evolution of HP/LT and LP/LT metasediments (see review of Bousquet et al. 2008; and references therein), accurate characterization of metamorphic gradients and P–T-paths still remains problematic. Classical petrology based on analysing coexisting mineral assemblages and applying equilibrium thermodynamics reaches its limits, particularly in rocks that experienced low-grade conditions. A potentially powerful tool for estimating paleotemperatures is the investigation of the evolution of natural carbonaceous material, i.e. organic matter.

The presented investigation demonstrates the great potential for using Raman spectroscopy of carbonaceous material in the context of a detailed petrological and structural study. This method is very powerful for determining the maximum temperatures reached during metamorphism. Provided that the sampling is uniformly dense over a large area, this method also yields three-dimensional information on temperature gradients in the field. Up to now, such detailed spatial information has only been locally available in the Central Alps, as revealed by mapping of three-dimensional isograd patterns on a local scale (e.g. Streckeisen and Wenk 1974; Fox 1975; Thompson 1976). Carbonaceous material (CM) is ubiquitous in metasedimentary rocks in the area of investigation. This method is based on the widely accepted notion that the continuous transformation of the crystalline structure of CM from disordered organic matter to fully ordered graphite (generally called graphitization; e.g. Teichmüller 1987) is mainly temperature-dependent. Hence, the structural order of CM as detected with Raman spectroscopy is expected to increase systematically with increasing temperature (e.g. Pasteris and Wopenka 1991; Yui et al. 1996) and indeed, the relationship between structural ordering and temperature has been calibrated as a reliable geothermometer (Beyssac et al. 2002a; Rahl et al. 2005). A key feature of this method is that graphitization is an irreversible thermal process, as supported by the observation that the degree of crystallinity of CM is irreversible (e.g. Beyssac et al. 2002a). Therefore, this geothermometer always reliably records the peak temperature reached by a rock specimen along its P–T-path (e.g. Beyssac et al. 2004, 2007; Bollinger et al. 2004; Rantitsch et al. 2004, 2005; Guedes et al. 2005; Rahl et al. 2005; Negro et al. 2006; Judik et al. 2008; Kribek et al. 2008; Angiboust et al. 2009; Gabalda et al. 2009; Rantitsch and Judik 2009; Aoya et al. 2010).

This study presents a first systematic, comprehensive investigation of the evolution of CM using Raman spectroscopy over a large area of the Central Alps at the northeastern rim of the Lepontine dome that is

characterized by high topographic gradients. The peak temperature distribution in maps and profiles covers a large volume of calcareous, organic-rich metasediments (generally referred to as Bündnerschiefer) that were deposited onto basement of the European continental margin and the adjacent Valais oceanic domain in Cretaceous time (Steinmann 1994; Berger et al. 2005; Wiederkehr et al. 2008). The dataset comprises a total of 214 samples (Figs. 1, 2, Table 1) and allows for high-resolution mapping of maximum metamorphic temperatures in three dimensions. Two different calibrations (Beyssac et al. 2002a; Rahl et al. 2005) were used and will be compared with each other in this study. The peak temperature distribution will be discussed in terms of the P–T-paths associated with the high-pressure and Barrow-type metamorphisms, respectively.

Geological setting and sampling strategy

The analysed Mesozoic metasediments are located partly within the northeastern rim of the Lepontine dome and partly in easterly adjacent areas (inset of Fig. 1). This working area turned out to be ideal for studying temperature gradients in a transition zone between realms that are characterized by collision- and subduction-related metamorphic overprints. The investigated zone of transition extends from the Garvera-Lukmanier-Pizzo Molare area in the W to the Prättigau half-window in the E and also includes the N–S-oriented Misox Zone located between the Adula and Tambo nappes (Figs. 1, 2). This allows for continuous observation of the same metasedimentary units along strike, i.e. from an area dominated by amphibolite-facies, Barrovian overprint in the SW to one dominated by blueschist-facies conditions in the NE (Fig. 1; Wiederkehr et al. 2008).

Tectono-metamorphic background

Within our working area, pre-Alpine basement nappes predominate over Mesozoic metasediments in the west and at deeper structural levels. These basement nappes formed by scraping off of uppermost crustal slices from the southward-subducting European margin and accreting them to the overlying Penninic nappe stack during the latest stages of Alpine plate convergence (Schmid et al. 1996). Because they structurally underlie the Penninic nappes formed by the remnants of two branches of Alpine Tethys and slices of an intervening Briançonnais microcontinent, they are referred to as Sub-Penninic (Milnes 1974; Froitzheim et al. 1996; Schmid et al. 2004). The basement nappes include, from bottom to top, the Gotthard, Lucomagno-Leventina, Simano and Adula nappes. Together, they form the bulk of the Lepontine structural dome that exposes the deepest tectonic units of the Alps. These basement nappes are overlain directly by thin slivers of Mesozoic metasediments that were part of the Mesozoic cover of this European margin (Europe-derived metasedimentary units of Figs. 1, 2). These Europe-derived metasediments are complexly folded and wrapped around the frontal parts of the Sub-Penninic basement nappes (e.g. Thakur 1973; Milnes 1974; Probst 1980).

The Penninic Basal Thrust separates the Europe-derived Sub-Penninic units from the Lower Penninic cover nappes and thrust slices that originated from the Valais Ocean (e.g. Steinmann 1994; Wiederkehr et al. 2008). The latter, referred to as Valaisan, consist almost exclusively of Mesozoic metasediments referred to as Bündnerschiefer (e.g. Probst 1980; Steinmann 1994; Berger et al. 2005; Figs. 1, 2). Because they constitute a structurally higher nappe stack with an axial plunge towards the east, they are predominantly found in the eastern parts of the studied area.

The northeastern margin of the Lepontine dome is the locus of several pioneering studies addressing fundamental principles related to the evolution of prograde Barrovian metamorphism (Niggli and Niggli 1965; Chadwick 1968; Frey 1969, 1978; Niggli 1970; Wenk 1970; Fox 1975; Livi et al. 2002). Metamorphic grade increases continuously from chloritoid- and margarite-bearing micaschists that are part of the greenschist-facies domain in the Urseren-Garvera Zone (Frey 1978; Livi et al. 2002) to staurolite-kyanite-garnet-biotite-bearing metasediments indicating amphibolite-facies conditions around the Lukmanier area and Pizzo Molare (Fig. 1; Chadwick 1968; Frey 1969; Thakur 1971; Fox 1975). Lower/middle amphibolite-facies metamorphic conditions (0.5–0.8 GPa and 500–550°C) have been estimated for Barrow-type metamorphism in the northeastern Lepontine dome (Chadwick 1968; Frey 1969; Fox 1975; Engi et al. 1995; Todd and Engi 1997; Frey and Ferreiro Mählmann 1999). A similar progressive increase in metamorphic conditions is also found in the Misox Zone further to the east (Thompson 1976; Teutsch 1982; Fig. 1).

Low-grade metasediments predominate in the area northeast of the Lepontine dome, but there the metamorphic record is ill-constrained due to the scarcity of unambiguous mineral assemblages; often one can only infer "greenschist-facies" conditions. However, the recognition of Fe–Mg carpholite in the metasediments of the Valaisan east of the Lepontine dome indicates that blueschist-facies conditions of 1.2–1.4 GPa and 350–400°C were established before the late-stage overprinting under greenschist-facies conditions (Fig. 1; Goffé and Oberhänsli 1992; Oberhänsli et al. 1995; Bousquet et al. 1998). The discovery of carpholite documented the existence of a second and northern subduction zone within the Valais oceanic

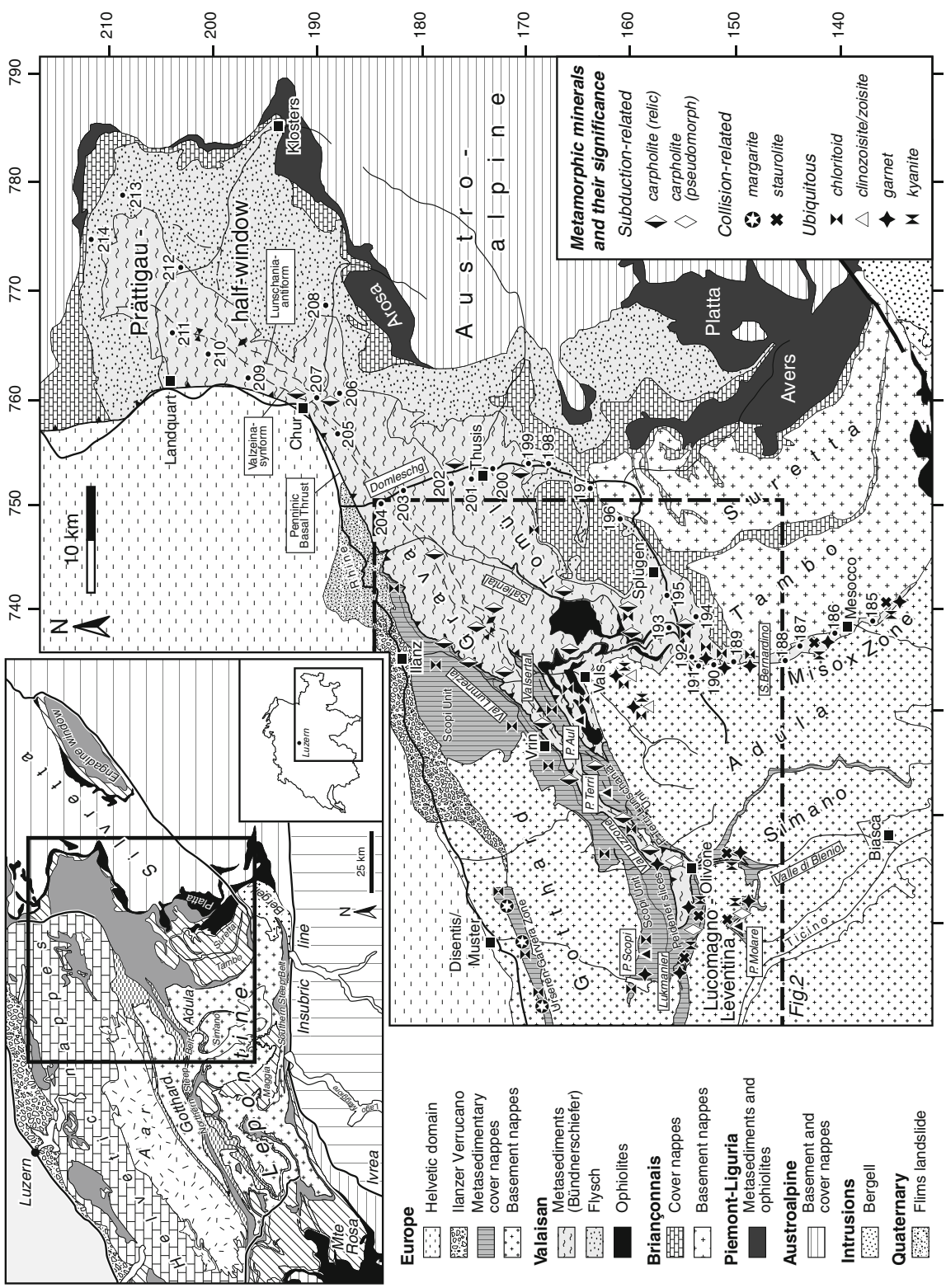

Fig. 1 Geological map of the investigated area indicating the main occurrences of minerals indicative for HP/LT metamorphism and Barrovian overprint, as well as the main geographical names mentioned in the text and giving the locations of specimen numbers 185–214; refer to Fig. 2 regarding the locations of all other samples and to Table 1 for exact location. The *dashed line* indicates the outlines of the more detailed map shown in Fig. 2. The tectonic map of the Central Alps in the *inset* (*upper left*) is after Schmid et al. (2004). Coordinates given are those of the Swiss maps

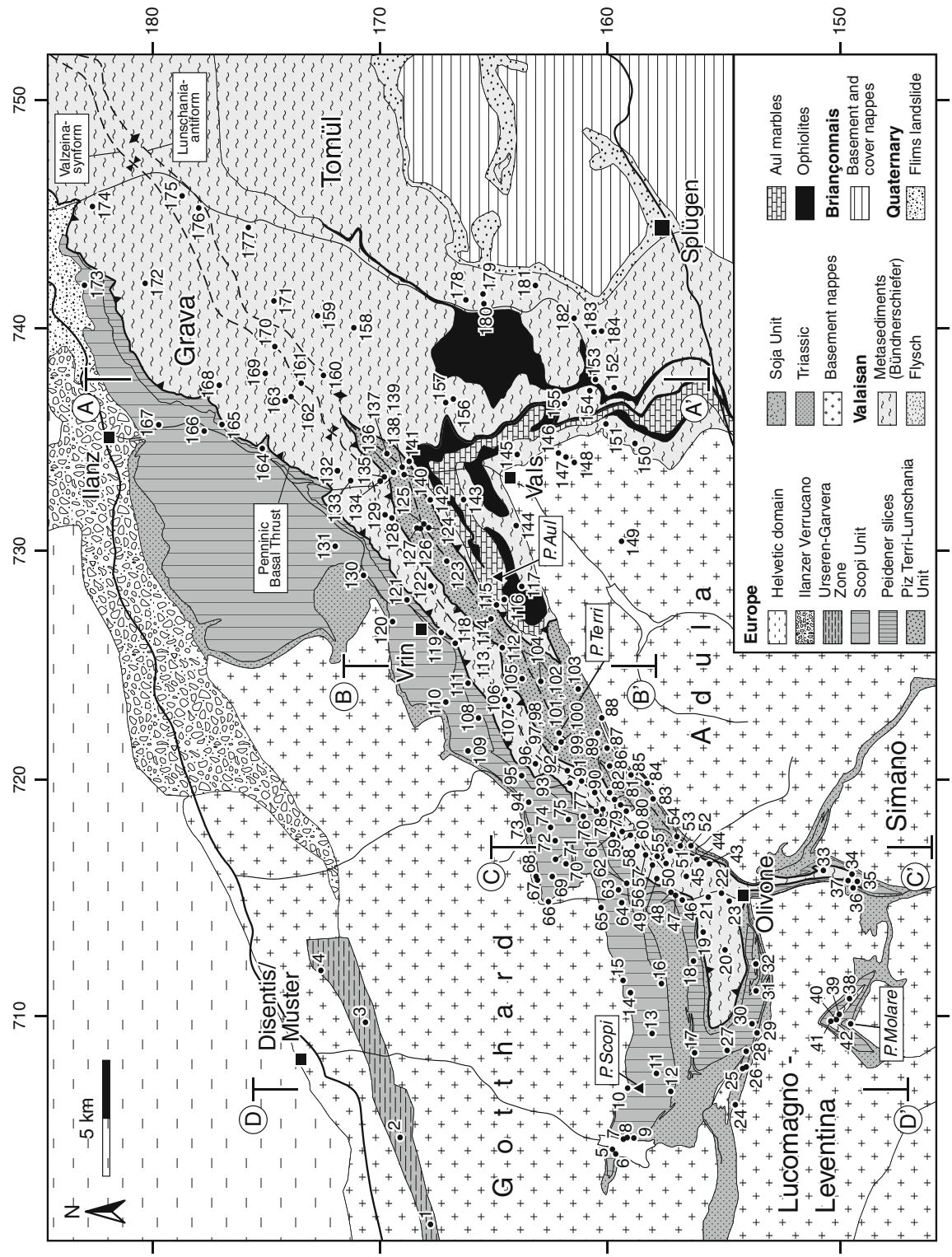

Fig. 2 Detailed geological map of the south-western part of the study area (see outlines of the map given in Fig. 1) showing the locations of specimen numbers 1–184; refer to Fig. 1 regarding the locations of all other samples and to Table 1 for exact location. The traces of cross-sections shown in Fig. 8b–e are indicated by the letters *A–A′*, *B–B′*, *C–C′* and *D–D′*, respectively. Coordinates given are those of the Swiss maps

Table 1 This list of samples also includes our own samples, completed by samples from the following studies: [(1)] Frey (1978); [(2)] Hoefs and Frey (1976); [(3)] Thoenen (1989); [(4)] Petrova et al. (2002); [(5)] Frey et al. (1982)

#	Sample name	Swiss map coordinates		Elev. (m)	Tect. unit	Mineral assemblage	# sp.	R1		R2		Beyssac et al. (2002)		Rahl et al. (2005)	
		X	Y					Mean	SD	Mean	SD	T (°C)	CI	T (°C)	CI
1	MF 856[(1)]	700′800	167′700	2220	UG	Ctd-Mrg-WM-Chl-Qtz	25	0.60	0.08	0.43	0.03	452	5	446	4
2	MF 898[(1)]	704′500	169′000	1580	UG	Ctd-Mrg-WM-Chl-Qtz	25	0.74	0.11	0.47	0.03	432	6	429	4
3	MF 120[(2)]	709′400	170′500	1420	UG	Ctd-Mrg-WM-Chl-Qtz	25	1.11	0.16	0.56	0.03	392	5	396	4
4	MF 922[(1)]	711′600	172′400	2220	UG	Ctd-Mrg-WM-Chl-Qtz	25	1.76	0.13	0.63	0.01	359	2	376	4
5	MF 153[(2)]	704′000	159′800	1930	S	Bt-Mrg-WM-Qtz	25	0.19	0.04	0.24	0.04	534	8	539	14
6	LUK 066	703′915	159′784	1930	S	Grt-Bt-Mrg-WM-Chl-Qtz-Cc/Do	15	0.20	0.02	0.26	0.02	525	4	521	5
7	MF 951[(3)]	704′513	159′622	1960	S	Grt-Bt-Zo/Czo-WM-Qtz-Cc/Do	25	0.19	0.03	0.25	0.03	532	5	533	9
8	LUK 069	704′453	159′166	1970	S	Plag-WM-Qtz-Cc/Do	15	0.19	0.01	0.25	0.01	532	3	533	6
9	MF 944[(2)]	704′500	158′900	2000	S	Bt-Plag-Zo/Czo-WM-Qtz-Cc/Do	30	0.20	0.03	0.25	0.03	528	5	527	9
10	BOV 0612	706′656	158′772	3190	S	Ctd-WM-Chl-Qtz	45	0.29	0.07	0.31	0.04	502	6	491	9
11	BOV 064	707′305	157′857	2910	S	Plag-WM-Chl-Qtz-Cc/Do	15	0.21	0.03	0.26	0.03	524	7	522	11
12	MF 184[(3)]	706′577	157′426	2520	S	Grt-Bt-Zo/Czo-WM-Qtz	30	0.18	0.03	0.24	0.03	535	5	538	9
13	BOV 063	709′067	158′045	2580	S	Plag-WM-Qtz-Cc/Do	25	0.26	0.04	0.30	0.03	508	6	496	10
14	BOV 067	710′904	159′018	2350	S	Ctd-WM-Chl-Qtz	25	0.33	0.06	0.34	0.03	491	6	475	9
15	BOV 068	711′421	159′354	2380	S	Ctd-WM-Chl-Qtz	25	0.32	0.06	0.33	0.03	494	6	478	9
16	BOV 0611	711′277	157′680	1890	S	Grt-Bt-Plag-Zo/Czo-WM-Chl-Qtz	15	0.20	0.03	0.26	0.02	524	5	519	9
17	DÖT 063	708′208	156′187	2530	PS	Grt-Bt-Zo/Czo-WM-Chl-Qtz	21	0.17	0.02	0.23	0.02	538	4	542	7
18	DÖT 061	712′281	156′242	2100	PS	Grt-Bt-Ctd-Mrg-WM-Qtz	15	0.17	0.03	0.22	0.02	542	6	551	9
19	DÖT 052	713′556	155′867	2099	G	Bt-Plag-Zo/Czo-WM-Qtz-Cc/Do	10	0.19	0.03	0.25	0.03	529	10	528	17
20	DÖT 0510	712′890	154′745	1465	G	Grt-Bt-Plag-Zo/Czo-WM-Qtz-Cc/Do	10	0.17	0.03	0.25	0.03	529	9	522	16
21	BLE 0512	715′112	155′757	1090	G	Bt-Plag-Zo/Czo-WM-Chl-Qtz-Cc/Do	19	0.17	0.04	0.23	0.05	538	10	544	18
22	BLE 056	715′097	154′882	980	G	Bt-Plag-Zo/Czo-WM-Chl-Qtz-Cc/Do	10	0.18	0.05	0.24	0.05	534	16	537	29
23	BLE 052	714′864	154′466	910	G	Bt-Plag-Zo/Czo-WM-Chl-Qtz-Cc/Do	31	0.18	0.05	0.24	0.05	535	8	539	15
24	MF 1575[(2)]	705′900	154′400	1840	PS	Ky-Bt-WM-Qtz	20	0.15	0.02	0.20	0.02	550	5	567	8
25	LUK 0630	707′475	154′073	1790	PS	Grt-Bt-Plag-Zo/Czo-WM-Qtz-Cc/Do	36	0.14	0.03	0.20	0.04	552	5	567	10
26	MF 1581[(2)]	707′500	154′000	1780	PS	St-Ky-Grt-Bt-Plag-WM-Chl-Qtz	25	0.14	0.04	0.20	0.05	553	8	570	16
27	LUK 0644	708′402	154′680	1820	PS	St-Grt-Bt-Plag-Zo/Czo-WM-Qtz	20	0.14	0.05	0.19	0.05	557	11	579	21
28	LUK 0641	708′254	153′917	1590	PS	St-Ky-Grt-Bt-Plag-Zo/Czo-WM-Chl-Qtz	10	0.14	0.03	0.20	0.04	553	13	569	23
29	MF 1606[(2)]	709′100	153′500	1470	PS	St-Grt-Bt-Plag-Zo/Czo-WM-Chl-Qtz	25	0.13	0.03	0.18	0.04	561	8	585	14
30	LUK 0637	709′495	153′619	1520	PS	St-Grt-Bt-Plag-Zo/Czo-WM-Chl-Qtz-Cc/Do	10	0.16	0.03	0.22	0.03	544	10	553	18
31	LUK 0635	710′870	153′442	1430	PS	Grt-Bt-Plag-Zo/Czo-WM-Qtz	20	0.14	0.03	0.19	0.04	555	8	574	15
32	LUK 0646	712′242	153′582	1340	PS	Grt-Bt-Plag-Zo/Czo-WM-Qtz-Cc/Do	20	0.15	0.02	0.20	0.02	550	5	565	9
33	GRU 061	716′288	150′576	770	G	Bt-Plag-Zo/Czo-WM-Chl-Qtz-Cc/Do	21	0.14	0.03	0.19	0.03	556	6	577	11

Table 1 continued

#	Sample name	Swiss map coordinates		Elev. (m)	Tect. unit	Mineral assemblage	# sp.	R1		R2		Beyssac et al. (2002)		Rahl et al. (2005)	
		X	Y					Mean	SD	Mean	SD	T (°C)	CI	T (°C)	CI
34	GRU 062	716′156	149′270	760	G	Bt-Plag-Zo/Czo-WM-Chl-Qtz-Cc/Do	10	0.12	0.03	0.18	0.03	559	11	579	19
35	GRU 057	715′621	148′504	700	G	Bt-Plag-WM-Qtz-Cc/Do	10	0.13	0.03	0.19	0.04	558	11	578	21
36	GRU 053	714′990	149′545	630	PS	St-Ky-Grt-Bt-Plag-WM-Chl-Qtz	22	0.12	0.04	0.17	0.06	564	11	589	20
37	GRU 058	715′734	149′305	750	G	Bt-Plag-WM-Qtz-Cc/Do	10	0.13	0.02	0.18	0.02	560	6	582	11
38	MOL 051	710′270	149′696	2270	PS	St-Ky-Grt-Bt-Plag-WM-Qtz	10	0.12	0.02	0.19	0.03	557	8	574	15
39	MOL 055	709′715	149′780	2400	G	Bt-WM-Qtz-Cc/Do	10	0.12	0.02	0.17	0.02	563	7	587	13
40	MOL 062	709′617	150′119	2450	PS	St-Grt-Bt-Plag-Zo/Czo-WM-Qtz	10	0.12	0.02	0.18	0.03	560	8	582	15
41	MOL 058	709′468	150′172	2550	G	Bt-WM-Qtz-Cc/Do	10	0.13	0.02	0.19	0.03	557	9	576	16
42	MOL 061	709′541	149′308	2310	PS	St-Ky-Grt-Bt-Plag-WM-Qtz	10	0.12	0.02	0.17	0.02	563	6	588	12
43	CAR 0516	716′440	155′418	1570	G	Bt-Plag-Zo/Czo-WM-Qtz-Cc/Do	15	0.23	0.06	0.28	0.05	518	12	512	20
44	**CAR 0515**	**716′834**	**156′093**	**1630**	**G**	**Bt-Plag-Zo/Czo-WM-Qtz-Cc/Do**	**16**	**0.14**	**0.07**	**0.19**	**0.08**	**558**	**19**	**580**	**34**
45	SOS 051	716′092	156′428	2160	G	Bt-Plag-Ttn-Zo/Czo-WM-Qtz	15	0.25	0.05	0.30	0.03	506	7	490	11
46	BLE 0410	715′029	156′841	1190	PS	Grt-Bt-Plag-Zo/Czo-Mrg-WM-Qtz-Cc/Do	14	0.20	0.04	0.26	0.04	526	10	522	16
47	BLE 061	715′186	157′232	1210	PS	Grt-Bt-WM-Chl-Qtz	22	0.21	0.03	0.27	0.03	522	6	516	10
48	BLE 0413	715′346	157′292	1230	PS	Bt-Plag-Ttn-Zo/Czo-WM-Qtz-Cc/Do	13	0.22	0.05	0.27	0.04	519	11	512	19
49	LUZ 0442	716′017	157′831	1390	G	Bt-Plag-Zo/Czo-WM-Qtz-Cc/Do	15	0.25	0.09	0.29	0.07	513	18	506	29
50	CAR 0517	716′596	157′598	1650	G	Plag-WM-Qtz-Cc/Do	16	0.26	0.07	0.29	0.05	511	12	503	18
51	**CAR 055**	**717′084**	**157′365**	**2030**	**G**	**Plag-Zo/Czo-WM-Chl-Qtz**	**16**	**0.20**	**0.06**	**0.25**	**0.04**	**532**	**9**	**536**	**15**
52	CAR 052	717′226	156′393	1680	TL	WM-Qtz-Cc/Do	16	0.27	0.06	0.30	0.05	507	11	494	18
53	CAR 0510	717′901	156′992	2140	TL	Ctd-WM-Chl-Qtz-Cc/Do	17	0.31	0.11	0.33	0.07	496	15	482	23
54	CAR 059	717′906	157′007	2160	TL	WM-Chl-Qtz-Cc/Do	10	0.38	0.06	0.38	0.03	474	9	448	13
55	CAR 0519	716′835	157′783	1580	G	Plag-WM-Chl-Qtz-Cc/Do	10	0.26	0.05	0.30	0.04	508	11	496	17
56	LUZ 0456	716′469	158′124	1450	G	Plag-Ttn-Zo/Czo-WM-Chl-Qtz-Cc/Do	17	0.24	0.07	0.29	0.06	514	14	505	22
57	LUZ 055	716′865	158′363	1780	G	Plag-Ttn-Zo/Czo-WM-Chl-Qtz	10	0.35	0.05	0.36	0.04	480	11	451	15
58	CAV 054	717′107	158′540	1770	G	Plag-Zo/Czo-WM-Chl-Qtz-Cc/Do	16	0.35	0.08	0.34	0.04	490	10	475	14
59	LUZ 051	717′825	159′166	1850	G	WM-Chl-Qtz-Cc/Do	10	0.33	0.06	0.34	0.03	489	11	468	15
60	CAV 0520	717′808	159′311	1870	G	Plag-WM-Qtz-Cc/Do	15	0.35	0.07	0.36	0.04	481	10	457	15
61	CAV 0511	717′618	159′926	1820	PS	WM-Qtz	16	0.35	0.06	0.35	0.04	485	9	464	13
62	CAM 062	715′474	159′346	1430	PS	WM-Chl-Qtz	15	0.26	0.05	0.31	0.04	504	9	486	15
63	CAM 065	715′367	159′595	1400	S	Plag-WM-Chl-Qtz-Cc/Do	25	0.31	0.05	0.33	0.04	496	7	480	10
64	CAM 066	714′841	159′482	1380	S	Plag-WM-Chl-Qtz-Cc/Do	22	0.30	0.03	0.32	0.02	498	4	483	7
65	CAM 069	714′624	160′457	1470	S	Ctd-WM-Chl-Qtz	18	0.36	0.05	0.37	0.03	478	6	452	10
66	GRE 051	714′727	162′889	2000	S	Ctd-WM-Chl-Qtz	25	0.44	0.05	0.39	0.03	468	5	447	6
67	GRE 052	715′664	163′152	2310	S	Ctd-WM-Chl-Qtz	15	0.43	0.04	0.38	0.02	474	5	460	7

Table 1 continued

#	Sample name	Swiss map coordinates		Elev. (m)	Tect. unit	Mineral assemblage	# sp.	R1		R2		Beyssac et al. (2002)		Rahl et al. (2005)	
		X	Y					Mean	SD	Mean	SD	T (°C)	CI	T (°C)	CI
68	GRE 061	715′971	163′212	2370	S	Ctd-WM-Chl-Qtz	22	0.45	0.08	0.38	0.04	471	7	457	10
69	GRE 0610	715′985	162′527	2660	S	Ctd-WM-Chl-Qtz	22	0.41	0.05	0.36	0.02	479	5	465	6
70	GRE 069	716′552	161′946	2790	S	Ctd-WM-Chl-Qtz	22	0.43	0.05	0.38	0.03	471	5	453	7
71	GRE 068	716′779	162′403	2730	S	Ctd-WM-Chl-Qtz	22	0.41	0.07	0.37	0.04	477	7	461	9
72	GRE 067	717′565	162′430	2790	S	Ctd-WM-Chl-Qtz	22	0.43	0.06	0.38	0.03	473	6	457	7
73	GRE 062	718′047	163′562	2320	S	Ctd-WM-Chl-Qtz	20	0.48	0.05	0.39	0.02	466	5	451	7
74	GRE 065	718′180	162′606	2590	S	Ctd-WM-Chl-Qtz	15	0.48	0.08	0.40	0.03	462	7	444	10
75	LAR 0612	718′524	161′805	2050	S	WM-Qtz-Cc/Do	10	0.50	0.07	0.41	0.03	460	9	443	11
76	LAR 0614	718′722	160′899	1840	PS	WM-Qtz-Cc/Do	15	0.53	0.06	0.41	0.02	458	6	445	7
77	LAR 056	718′780	160′815	1870	PS	WM-Chl-Qtz-Cc/Do	10	0.34	0.07	0.35	0.04	486	14	464	20
78	LAR 0615	718′783	160′426	1790	G	WM-Chl-Qtz	18	0.49	0.04	0.43	0.02	448	4	412	6
79	MOT 0514	718′843	159′290	1670	TL	WM-Qtz-Cc/Do	11	0.36	0.05	0.39	0.03	480	11	456	17
80	GAR 055	719′017	159′367	1680	TL	Ctd-WM-Chl-Qtz	10	0.41	0.06	0.39	0.02	468	8	439	10
81	LUZ 0423	719′240	159′596	1780	TL	WM-Qtz-Cc/Do	20	0.40	0.08	0.39	0.04	468	9	436	12
82	GAR 054	719′645	159′991	1850	TL	WM-Chl-Qtz-Cc/Do	10	0.41	0.07	0.39	0.03	470	11	443	14
83	SCA 052	719′402	158′089	1790	TL	WM-Qtz-Cc/Do	11	0.35	0.06	0.36	0.03	482	10	458	15
84	**SCA 051**	**720′104**	**158′455**	**2270**	**TL**	**WM-Qtz-Cc/Do**	**10**	**0.30**	**0.05**	**0.32**	**0.03**	**500**	**9**	**489**	**12**
85	SCA 071	720′417	159′022	2540	TL	WM-Chl-Qtz-Cc/Do	20	0.43	0.04	0.40	0.02	465	5	437	8
86	**GAR 053**	**720′863**	**159′895**	**2060**	**TL**	**Ctd-WM-Chl-Qtz-Cc/Do**	**10**	**0.29**	**0.04**	**0.32**	**0.02**	**499**	**8**	**485**	**12**
87	GAR 052	721′604	160′190	2210	TL	Ctd-WM-Chl-Qtz-Cc/Do	12	0.44	0.11	0.40	0.05	465	14	440	17
88	VRI 0622	722′939	160′396	2940	TL	Ctd-WM-Chl-Qtz-Cc/Do	23	0.72	0.09	0.46	0.03	438	5	439	4
89	GAR 056	722′366	160′378	2600	TL	WM-Qtz-Cc/Do	11	0.46	0.07	0.40	0.02	461	7	435	8
90	MOT 0513	719′622	160′641	1790	G	WM-Qtz-Cc/Do	16	0.50	0.13	0.40	0.06	461	14	445	16
91	MOT 0512	720′114	161′192	2090	G	WM-Chl-Qtz-Cc/Do	15	0.49	0.09	0.41	0.04	460	10	440	12
92	LUZ 0425	720′598	161′470	2290	G	WM-Chl-Qtz	15	0.48	0.07	0.40	0.02	461	6	440	6
93	MOT 051	719′927	161′888	2210	G	WM-Chl-Qtz-Cc/Do	15	0.51	0.08	0.41	0.04	461	9	447	11
94	GRE 063	719′274	163′604	2250	S	Ctd-WM-Chl-Qtz	22	0.49	0.07	0.41	0.03	460	7	441	8
95	MOT 053	720′455	163′705	2420	PS	Ctd-WM-Chl-Qtz	22	0.50	0.10	0.40	0.04	464	8	452	9
96	MOT 059	720′730	163′126	2590	G	WM-Chl-Qtz-Cc/Do	16	0.62	0.11	0.44	0.04	445	8	435	7
97	**TER 0511**	**721′621**	**162′296**	**2750**	**TL**	**Ab-WM-Qtz**	**16**	**0.25**	**0.05**	**0.27**	**0.03**	**521**	**8**	**525**	**11**
98	TER 0510	721′682	162′126	2900	TL	WM-Qtz-Cc/Do	20	0.56	0.13	0.42	0.04	452	9	439	10
99	TER 058	721′830	162′118	2970	TL	WM-Chl-Qtz-Cc/Do	17	0.58	0.08	0.43	0.03	448	7	434	7
100	TER 057	721′991	162′147	3020	TL	WM-Chl-Qtz-Cc/Do	18	0.55	0.10	0.42	0.04	454	8	442	9
101	TER 056	722′082	162′198	3076	TL	WM-Qtz-Cc/Do	18	0.47	0.08	0.39	0.03	466	7	452	7

Table 1 continued

#	Sample name	Swiss map coordinates		Elev. (m)	Tect. unit	Mineral assemblage	# sp.	R1		R2		Beyssac et al. (2002)		Rahl et al. (2005)	
		X	Y					Mean	SD	Mean	SD	T (°C)	CI	T (°C)	CI
102	TER 051	722′245	162′212	3150	TL	WM-Qtz-Cc/Do	16	0.62	0.07	0.44	0.02	444	6	432	7
103	VRI 0618	724′214	161′412	2480	TL	WM-Qtz-Cc/Do	25	0.58	0.06	0.43	0.02	451	4	441	6
104	VRI 0616	724′498	162′815	1890	TL	WM-Qtz-Cc/Do	39	0.63	0.15	0.44	0.06	446	9	439	9
105	VRI 0629	724′661	163′907	2260	TL	WM-Qtz-Cc/Do	10	0.58	0.06	0.42	0.02	456	5	452	5
106	VRI 0630	723′747	164′637	2450	G	WM-Chl-Qtz	18	0.63	0.08	0.43	0.03	451	6	452	5
107	VRI 0633	723′227	164′617	2430	G	Ctd-WM-Chl-Qtz	22	0.59	0.12	0.43	0.04	450	9	439	10
108	VRI 061	722′919	165′841	2110	S	Ctd-WM-Chl-Qtz	20	0.65	0.08	0.43	0.02	450	5	453	4
109	VRI 064	721′495	166′274	2430	S	Ctd-WM-Chl-Qtz	17	0.64	0.17	0.42	0.05	454	12	458	11
110	VRI 0614	723′645	167′250	1870	S	Ctd-WM-Chl-Qtz	15	0.71	0.10	0.45	0.03	442	7	447	6
111	VRI 068	724′447	166′316	1630	PS	Ctd-WM-Chl-Qtz	15	0.67	0.08	0.45	0.02	442	5	437	6
112	VRI 052	726′018	164′498	1630	TL	WM-Qtz-Cc/Do	15	0.77	0.08	0.48	0.02	428	5	424	4
113	VRI 0636	727′363	165′266	2060	TL	WM-Qtz-Cc/Do	25	0.74	0.09	0.46	0.03	437	5	440	4
114	VRI 0637	727′363	165′266	2060	TL	WM-Qtz-Cc/Do	21	0.79	0.08	0.47	0.02	430	5	434	4
115	**VRI 0638**	**727′890**	**165′007**	**2250**	**G**	**WM-Qtz-Cc/Do**	**18**	**0.58**	**0.07**	**0.40**	**0.02**	**461**	**5**	**464**	**6**
116	VRI 0639	728′153	164′660	2520	AV	WM-Chl-Qtz	21	0.76	0.06	0.47	0.01	434	3	437	4
117	VRI 0640	728′577	164′464	2670	AV	Ab-WM-Chl-Qtz-Cc/Do	31	0.73	0.17	0.46	0.05	436	8	435	7
118	VRI 051	726′304	166′805	1420	G	WM-Qtz-Cc/Do	20	0.85	0.13	0.49	0.04	424	8	429	9
119	VRI 075	726′579	167′357	1400	PS	Ctd-WM-Chl-Qtz	25	0.72	0.10	0.46	0.02	436	4	435	3
120	VRI 073	727′048	169′497	1500	S	WM-Chl-Qtz-Cc/Do	25	0.95	0.12	0.52	0.02	408	4	411	2
121	VRI 0641	728′023	169′054	1280	PS	WM-Qtz-Cc/Do	22	0.80	0.19	0.47	0.04	431	8	436	6
122	VRI 0645	728′683	167′957	1570	G	WM-Chl-Qtz-Cc/Do	25	0.72	0.10	0.47	0.02	432	4	424	3
123	VRI 0649	729′844	167′225	2120	TL	WM-Qtz-Cc/Do	21	0.85	0.07	0.49	0.02	424	3	431	3
124	VAL 062	731′316	168′000	2420	TL	WM-Chl-Qtz	21	0.86	0.08	0.49	0.02	424	4	434	3
125	VAL 061	731′491	168′208	2270	TL	WM-Qtz-Cc/Do	26	0.95	0.16	0.52	0.03	410	6	412	8
126	VAL 063	731′289	168′354	2340	TL	WM-Chl-Qtz	24	0.76	0.09	0.48	0.02	426	4	419	4
127	VAL 064	731′289	168′557	2340	TL	WM-Chl-Qtz	18	0.74	0.07	0.46	0.02	437	4	440	4
128	VAL 066	731′805	169′620	2050	G	WM-Chl-Qtz-Cc/Do	20	0.84	0.12	0.49	0.03	421	6	422	6
129	VAL 065	731′823	169′913	2050	G	WM-Chl-Qtz-Cc/Do	19	0.90	0.11	0.50	0.02	418	5	425	5
130	VRI 072	729′104	170′789	1260	S	Ctd-WM-Chl-Qtz	25	1.00	0.13	0.53	0.02	405	4	409	4
131	VRI 0651	730′151	172′057	1370	S	Ctd-WM-Chl-Qtz	22	1.39	0.13	0.58	0.02	381	3	403	3
132	VAL 0546	733′770	171′970	1160	G	WM-Chl-Qtz-Cc/Do	16	1.21	0.08	0.57	0.01	389	4	402	4
133	VAL 0719	733′311	171′359	1020	G	WM-Chl-Qtz-Cc/Do	25	1.01	0.13	0.53	0.02	405	5	412	3
134	VAL 052	733′254	170′168	1050	G	WM-Qtz-Cc/Do	16	0.84	0.07	0.50	0.02	421	4	422	4
135	VAL 0720	733′422	169′874	1080	G	WM-Chl-Qtz-Cc/Do	27	0.88	0.13	0.51	0.03	416	6	416	5

Table 1 continued

#	Sample name	Swiss map coordinates		Elev. (m)	Tect. unit	Mineral assemblage	# sp.	R1		R2		Beyssac et al. (2002)		Rahl et al. (2005)	
		X	Y					Mean	SD	Mean	SD	T (°C)	CI	T (°C)	CI
136	**VAL 057**	**733′765**	**169′471**	**1100**	**TL**	**Ab-WM-Qtz-Cc/Do**	**16**	**0.35**	**0.07**	**0.33**	**0.03**	**496**	**8**	**492**	**10**
137	VAL 0624	734′691	169′923	1550	TL	WM-Chl-Qtz-Cc/Do	18	1.08	0.06	0.54	0.01	402	2	417	2
138	VAL 055	734′054	169′284	1100	TL	WM-Chl-Qtz-Cc/Do	17	0.88	0.12	0.50	0.03	417	7	418	5
139	**VAL 056**	**734′054**	**169′284**	**1100**	**TL**	**Ab-WM-Qtz-Cc/Do**	**19**	**0.48**	**0.14**	**0.38**	**0.06**	**472**	**12**	**465**	**14**
140	**VAL 067**	**733′620**	**169′160**	**1100**	**TL**	**WM-Chl-Qtz-Cc/Do**	**21**	**0.67**	**0.09**	**0.44**	**0.02**	**444**	**5**	**444**	**4**
141	VAL 0716	734′183	168′768	1180	G	WM-Chl-Qtz-Cc/Do	25	0.92	0.09	0.52	0.02	411	4	413	3
142	VAL 0714	732′470	167′831	2000	G	WM-Chl-Qtz-Cc/Do	25	0.93	0.13	0.52	0.03	411	5	412	3
143	VAL 0711	732′486	166′320	1950	AV	Ctd-WM-Chl-Qtz-Cc/Do	27	0.94	0.13	0.52	0.02	408	4	406	3
144	VAL 0710	731′370	163′971	1960	AV	Ctd-WM-Chl-Qtz-Cc/Do	25	0.87	0.09	0.51	0.02	416	4	415	3
145	VAL 0715	734′484	163′945	1750	AV	WM-Chl-Qtz-Cc/Do	26	0.94	0.07	0.52	0.02	410	3	414	3
146	**VAL 079**	**734′426**	**161′844**	**1740**	**AM**	**Grt-Zo/Czo-WM-Chl-Qtz-Cc/Do**	**20**	**0.24**	**0.06**	**0.29**	**0.04**	**511**	**8**	**499**	**12**
147	**VAL 078**	**734′383**	**161′757**	**1790**	**AM**	**Grt-Ctd-Zo/Czo-WM-Chl-Qtz-Cc/Do**	**30**	**0.24**	**0.05**	**0.29**	**0.05**	**511**	**8**	**497**	**13**
148	**VAL 076**	**734′248**	**161′383**	**1920**	**AM**	**Grt-Ctd-Zo/Czo-WM-Chl-Qtz-Cc/Do**	**22**	**0.20**	**0.05**	**0.27**	**0.05**	**522**	**10**	**513**	**18**
149	**VAL 072**	**730′645**	**159′313**	**2540**	**AM**	**Ky-Grt-Ctd-Zo/Czo-WM-Chl-Qtz-Cc/Do**	**27**	**0.22**	**0.05**	**0.28**	**0.05**	**515**	**8**	**503**	**14**
150	VAL 0724	734′965	158′690	2300	AV	Ab-WM-Chl-Qtz-Cc/Do	25	0.71	0.09	0.47	0.03	432	5	424	5
151	VAL 0722	735′836	160′005	1970	AV	Ab-WM-Chl-Qtz-Cc/Do	25	0.89	0.10	0.51	0.02	413	3	413	3
152	VAL 0618	737′462	159′815	2930	T	WM-Chl-Qtz	18	1.18	0.10	0.55	0.01	397	3	418	2
153	VAL 0617	737′821	160′646	2640	T	Ab-WM-Chl-Qtz	18	1.20	0.12	0.55	0.02	396	5	418	4
154	VAL 0615	737′312	160′904	2470	G	WM-Chl-Qtz-Cc/Do	18	1.18	0.12	0.55	0.02	397	5	416	4
155	VAL 0614	736′748	162′002	2330	G	Ab-WM-Chl-Qtz-Cc/Do	18	1.21	0.09	0.56	0.01	393	3	413	2
156	VAL 0610	736′953	166′914	2020	G	WM-Chl-Qtz-Cc/Do	18	1.37	0.16	0.58	0.02	384	4	406	3
157	VAL 0611	736′582	167′233	2040	G	WM-Chl-Qtz-Cc/Do	18	1.33	0.13	0.57	0.02	387	4	410	3
158	SAF 072	740′135	171′221	2460	G	WM-Chl-Qtz	25	1.58	0.19	0.62	0.02	365	4	379	4
159	SAF 071	740′657	172′842	2590	G	WM-Chl-Qtz	25	1.58	0.16	0.62	0.02	367	4	383	4
160	VAL 0561	737′954	172′752	1440	G	WM-Chl-Qtz-Cc/Do	25	1.06	0.07	0.54	0.01	399	2	407	2
161	VAL 0574	737′710	173′714	1440	G	WM-Chl-Qtz-Cc/Do	25	1.09	0.09	0.55	0.01	395	3	402	2
162	VAL 0578	736′964	174′114	1390	G	WM-Qtz-Cc/Do	18	1.19	0.14	0.56	0.03	390	6	401	5
163	VAL 0580	736′871	174′310	1370	G	Cp-WM-Chl-Qtz-Cc/Do	20	1.21	0.13	0.56	0.02	390	4	404	2
164	VAL 0718	734′668	175′467	820	PS	Ctd-WM-Chl-Qtz	25	1.76	0.16	0.63	0.02	359	3	375	5
165	VAL 0731	735′717	177′200	860	PS	Ctd-WM-Chl-Qtz	25	1.52	0.11	0.61	0.01	371	2	390	3
166	VRI 0652	735′316	177′958	1070	S	Ctd-WM-Chl-Qtz	22	2.02	0.20	0.65	0.02	353	3	364	8
167	VAL 0717	735′693	179′872	740	S	Ctd-WM-Chl-Qtz	25	2.04	0.13	0.66	0.01	348	2	352	5
168	VAL 0729	737′575	177′229	1320	G	WM-Chl-Qtz-Cc/Do	30	1.43	0.09	0.60	0.01	376	2	396	2
169	VAL 0726	738′102	175′160	1580	G	WM-Chl-Qtz-Cc/Do	25	1.58	0.12	0.61	0.01	368	2	387	3

Table 1 continued

#	Sample name	Swiss map coordinates		Elev. (m)	Tect. unit	Mineral assemblage	# sp.	R1		R2		Beyssac et al. (2002)		Rahl et al. (2005)	
		X	Y					Mean	SD	Mean	SD	T (°C)	CI	T (°C)	CI
170	VAL 0727	739′267	174′747	1770	G	WM-Chl-Qtz-Cc/Do	30	1.25	0.11	0.57	0.02	386	3	400	2
171	SAF 073	741′354	174′746	2470	G	WM-Chl-Qtz-Cc/Do	25	1.51	0.12	0.61	0.01	369	2	384	2
172	VAL 0619	741′880	180′573	1330	G	WM-Chl-Qtz-Cc/Do	16	1.93	0.21	0.64	0.02	354	5	365	10
173	SAF 0723	741′859	183′102	820	S	Ctd-WM-Chl-Qtz-Cc/Do	30	1.93	0.17	0.66	0.02	348	4	350	8
174	SAF 0715	745′396	182′715	1030	G	WM-Chl-Qtz-Cc/Do	25	1.76	0.15	0.64	0.01	356	3	367	6
175	SAF 0527	746′016	178′803	1300	G	Cp-WM-Chl-Qtz-Cc/Do	15	1.62	0.16	0.62	0.02	364	4	380	6
176	SAF 0713	745′462	178′127	1300	G	WM-Chl-Qtz-Cc/Do	30	1.76	0.14	0.64	0.02	356	3	367	5
177	SAF 0712	744′572	175′876	1290	G	WM-Chl-Qtz-Cc/Do	30	1.48	0.07	0.61	0.01	369	2	382	2
178	SAF 0517	741′595	166′949	1700	T	WM-Chl-Qtz-Cc/Do	16	1.49	0.11	0.61	0.01	372	3	389	3
179	SAF 0511	741′585	166′188	1700	T	Ctd-WM-Chl-Qtz-Cc/Do	15	1.52	0.19	0.61	0.02	372	6	390	6
180	SAF 054	740′977	165′568	1700	T	WM-Chl-Qtz_Cc/Do	15	1.35	0.12	0.58	0.02	382	4	400	4
181	SAF 0722	741′959	163′126	1930	T	WM-Chl-Qtz-Cc/Do	25	1.17	0.09	0.57	0.01	389	3	398	2
182	SAF 0711	740′451	161′298	2240	T	Ctd-WM-Chl-Qtz-Cc/Do	25	1.16	0.08	0.55	0.01	396	3	413	3
183	SAF 0718	739′942	160′530	2350	T	WM-Chl-Qtz	25	1.09	0.10	0.55	0.02	398	3	408	3
184	SAF 075	739′980	160′207	2490	T	WM-Chl-Qtz	26	1.07	0.09	0.53	0.02	404	3	419	3
185	MF 2141[4]	738′300	137′025	1200	M	Grt-Bt-Plag-WM-Chl-Qtz	35	0.17	0.04	0.23	0.05	541	7	548	13
186	MF 2042[4]	737′600	140′450	900	M	Grt-Plag-WM-Chl-Qtz	23	0.20	0.05	0.25	0.04	532	8	535	13
187	MF 1872[5]	736′300	143′800	1240	M	Mrg-WM-Chl-Qtz-Cc/Do	20	0.39	0.11	0.36	0.06	480	12	461	18
188	MF 1895[4]	734′900	145′325	1850	M	Grt-Plag-WM-Chl-Qtz	25	0.30	0.02	0.33	0.02	493	3	472	6
189	TP 32[4]	734′750	150′350	2220	M	Ctd-Zo/Czo-WM-Chl-Qtz-Cc/Do	23	0.31	0.04	0.34	0.02	490	4	467	5
190	**TP 31[4]**	**734′600**	**152′200**	**2120**	**M**	**Grt-Ctd-Zo/Czo-WM-Qtz-Cc/Do**	**25**	**0.23**	**0.04**	**0.28**	**0.03**	**516**	**6**	**508**	**10**
191	**TP 34[4]**	**734′450**	**153′600**	**1840**	**M**	**Grt-Ctd-Zo/Czo-WM-Chl-Qtz-Cc/Do**	**25**	**0.23**	**0.03**	**0.29**	**0.03**	**512**	**5**	**498**	**8**
192	TP 25[4]	735′325	154′200	1800	M	Ab-WM-Chl-Qtz-Cc/Do	17	0.49	0.04	0.41	0.01	460	3	441	4
193	TP 24[4]	738′125	156′475	1770	G	WM-Chl-Qtz-Cc/Do	25	0.70	0.10	0.46	0.03	438	5	437	4
194	HINT 079	739′193	153′874	1670	T	Cp-Ctd-WM-Chl-Qtz-Cc/Do	25	0.68	0.09	0.45	0.03	441	5	439	4
195	TP 22[4]	741′225	156′675	1620	T	Ab-WM-Chl-Qtz	25	0.96	0.07	0.52	0.02	409	3	416	4
196	TP 36[4]	748′700	161′350	2040	T	WM-Chl-Qtz	25	1.51	0.23	0.60	0.02	372	4	389	4
197	TP 37[4]	752′000	164′050	1000	T	WM-Chl-Qtz-Cc/Do	25	2.39	0.11	0.68	0.00	337	1	314	4
198	TP 20[4]	753′775	168′025	900	T	WM-Chl-Qtz-Cc/Do	20	1.99	0.08	0.65	0.01	351	2	360	4
199	TP 19[4]	753′800	169′925	870	T	WM-Chl-Qtz-Cc/Do	25	1.52	0.12	0.61	0.02	371	3	391	3
200	TP 15[4]	753′300	173′325	700	T	WM-Chl-Qtz	20	1.45	0.08	0.60	0.01	376	2	398	3
201	TP 39[4]	752′350	175′350	760	T	WM-Chl-Qtz-Cc/Do	20	1.53	0.16	0.60	0.01	374	3	397	3
202	TP 40[4]	751′850	177′300	670	T	WM-Chl-Qtz-Cc/Do	20	1.71	0.14	0.62	0.02	363	3	382	5
203	TP 12[4]	751′275	181′750	630	G	Ab-WM-Chl-Qtz-Cc/Do	21	1.63	0.10	0.62	0.01	364	2	382	3

Table 1 continued

#	Sample name	Swiss map coordinates		Elev. (m)	Tect. unit	Mineral assemblage	# sp.	R1		R2		Beyssac et al. (2002)		Rahl et al. (2005)	
		X	Y					Mean	SD	Mean	SD	T (°C)	CI	T (°C)	CI
204	TP 11[(4)]	750′150	183′600	680	G	WM-Chl-Qtz-Cc/Do	20	1.83	0.12	0.64	0.01	357	3	374	6
205	TP 9[(4)]	756′850	188′100	1030	G	WM-Chl-Qtz-Cc/Do	20	2.06	0.05	0.66	0.01	349	1	356	3
206	MW 9664[(4)]	760′650	187′870	800	G	WM-Chl-Qtz-Cc/Do	20	2.23	0.13	0.67	0.02	343	3	336	10
207	TP 42[(4)]	760′250	190′050	610	G	WM-Chl-Qtz-Cc/Do	15	2.09	0.19	0.66	0.01	346	3	345	8
208	Ps 7[(4)]	768′940	189′195	1200	PF	WM-Qtz-Cc/Do	10	1.24	0.12	>0.70		<330		255	5
209	TP 7[(4)]	762′125	196′500	970	G	WM-Chl-Qtz-Cc/Do	15	1.95	0.11	0.66	0.01	348	3	353	6
210	**TP 5[(4)]**	**764′375**	**200′300**	**1060**	**G**	**WM-Chl-Qtz**	**22**	**1.42**	**0.17**	**0.59**	**0.02**	**378**	**4**	**398**	**4**
211	Vs 3[(4)]	766′345	203′635	1250	G	WM-Qtz-Cc/Do	10	1.42	0.07	>0.70		<330		268	8
212	TP 1[(4)]	772′575	202′825	690	G	WM-Chl-Qtz-Cc/Do	12	1.47	0.06	>0.70		<330		266	6
213	MF 2987[(4)]	779′400	208′700	1830	PF	WM-Chl-Qtz-Cc/Do	10	0.56	0.02	>0.70		<330		131	5
214	MF 2986[(4)]	775′300	211′700	2150	PF	WM-Chl-Qtz-Cc/Do	10	0.55	0.02	>0.70		<330		135	6

The specimens were taken from the Valaisan and the Europe-derived metasedimentary units and analysed by Raman spectroscopy of carbonaceous material in this study. The specimen numbers corresponds with those whose location is shown in map and profile view (Figs. 1, 2, 8), the coordinates are the Swiss map coordinates. Elevation is given in meters. The origin of the samples (Tectonic Unit) is also given, whereby: UG = Urseren-Garvera Zone, S = Scopi Zone, PS = Peidener slices, TL = Piz Terri-Lunschania Unit, G = Grava nappe, T = Tomül nappe, M = Misox Zone, AV = Aul and Valser slices, PF= Prättigau Flysch, AM = internal Mesozoic of the Adula nappe complex. Also listed are observed mineral assemblage (mineral abbreviations used: *Ab* albite, *Bt* biotite, *Cc/Do* calcite/dolomite, *Chl* chlorite, *Cp* Fe-Mg carpholite, *Ctd* chloritoid, *Grt* garnet, *Ky* kyanite, *Mrg* margarite, *Plag* plagioclase, *St* staurolite, *Ttn* titanite/sphene, *WM* white mica, *Qtz* quartz, *Zo/Czo* zoisite/clinozoisite), number of recorded Raman spectra (# sp.), R1 and R2 ratio (mean value and standard deviation SD), RSCM-inferred mean temperature and uncertainty given for the 95% confidence interval (CI) for both calibrations. Temperature uncertainty was determined by dividing the standard deviation of the measurements by the square root of the number of measurements, multiplied by a parameter depending on the number of measurements as well as the chosen confidence interval. Samples highlighted by bold letters were not considered for the isotemperature contours (see text for "Discussion")

domain, located between units derived from the Briançonnais micro-continent and those derived from the distal European margin (e.g. Oberhänsli 1994). The trace of this subduction zone is again found in the carpholite-bearing HP/LT Petit St. Bernard Unit located southwest of the Lepontine dome (Goffé and Bousquet 1997; Bousquet et al. 2002; Loprieno et al. 2010). This HP/LT belt marks the suture of the Valais Ocean and is separated from a second more southerly located suture of the Piemont-Liguria Ocean also marked by a well-established HP-belt. The Briançonnais-derived nappes, which partly lack a high-pressure overprint (Frey and Ferreiro Mählmann 1999; Engi et al. 2004), separate these two HP/LT belts from each other.

The subduction-related blueschist-facies overprint, as well as the subsequent greenschist-facies retrogression in the NE part of the investigated area, pre-date an entirely separate collision-related, Barrow-type amphibolite-facies metamorphic overprint that is only developed in the southwestern part of the investigated area (see e.g. Wiederkehr et al. 2008). The two events were diachronous at the scale of the Alpine orogen and hence all indicators of metamorphic zoning such as peak-metamorphic temperature inferred by the present study must be diachronous as well (e.g. Hunziker et al. 1992; Brouwer et al. 2005; Wiederkehr et al. 2009). Diachronism is well documented by recent isotopic investigations. These report 42–40 Ma for the timing of HP-metamorphism of metasediments belonging to the Valaisan northeast of the Lepontine dome (Wiederkehr et al. 2009). Towards the southwest, this HP-event was subsequently overprinted by a surprisingly young amphibolite-facies Barrow-type metamorphic event affecting the northern part of the Lepontine thermal dome, recently dated to be younger than 20 Ma (Allaz 2008; Janots et al. 2009; Wiederkehr et al. 2009). Note that the earlier HP/LT metamorphism not only affected the metasediments of the Valaisan but also parts of the metasedimentary units derived from the European margin (i.e. Peidener slices and Piz Terri-Lunschania Unit; Figs. 1, 2; Wiederkehr et al. 2008; Derungs 2008; Wiederkehr 2009). This first metamorphic event is separated structurally from the second MP/MT Barrovian overprint by at least two deformational events, which results in a typically bimodal P–T-path (Brouwer et al. 2005; Zulbati 2008; Wiederkehr et al. 2008).

Sediments derived from the distal European margin (Sub-Penninic cover nappes and slices)

The sediments originally deposited onto the former distal European margin include the Urseren-Garvera Zone, the Scopi Unit and Peidener slices that together form the so-called Gotthard Mesozoic units as well as the Piz Terri-Lunschania Unit (Figs. 1, 2; see Wiederkehr et al. 2008 for further details). In general, these sedimentary slices are made up of a Triassic sequence consisting of quartzite, dolomitic marble, evaporite, metapelite and metamarl followed by a lower to middle Jurassic sequence of shale, sandstone, limestone, carbonaceous metapelite and calcschist; the latter often resemble the so-called Bündnerschiefer units derived from the Valais Ocean (Baumer et al. 1961; Probst 1980; Etter 1987; Berger et al. 2005). Jurassic-age black shale, marl and calcschist with a high content in CM were selected for sampling.

We also sampled Mesozoic metasediments found inside the northern basement-dominated Adula nappe complex (so-called "internal Mesozoic"; Löw 1987; sampling points depicted in Fig. 2 within the Adula nappe complex). These sediments consist of Triassic quartzite, dolomitic marble and evaporite that were sliced and imbricated with the Adula crystalline basement. Kyanite-chloritoid-garnet-zoisite/clinozoisite-bearing metamarl and calcschist of probably Lower Jurassic age are unambiguously associated with these Triassic sediments in some rare outcrops (Fig. 1; Jenny et al. 1923; Van der Plaas et al. 1958; Löw 1987; Thüring 1990; Wyss and Isler 2007). Given their strong lithological affinity with the metasediments found in the Scopi Unit, we also attribute these occurrences to the sediments scraped off of the distal European margin.

Sediments derived from the Valais Ocean (Lower Penninic cover nappes and slices)

Sediments derived from the predominantly oceanic Valais realm form voluminous and rather monotonous sequences of calcschist (Bündnerschiefer) thrust along the Penninic Basal Thrust onto the sediments of the former European margin. These Bündnerschiefer, together with flysch units, marbles and ophiolitic occurrences that are also part of the Valaisan, are subdivided into a number of tectonic units. The largest are the Grava nappe (including the Prättigau Flysch) and the Tomül nappe (Figs. 1, 2), both consisting of Cretaceous- to Eocene-age calcschist, limestone, shale, marl and sandy limestone (Nänny 1948; Ziegler 1956; Steinmann 1994). The existence of mafic and ultramafic rocks (Nabholz 1945) indicates that at least parts of the Valaisan Bündnerschiefer were deposited on oceanic crust (Steinmann 1994; Steinmann and Stille 1999). Some of the samples analysed come from the Misox Zone, a narrow zone of Mesozoic metasediments that also includes ophiolitic slices (e.g. Steinmann 1994). This zone is located between the Adula nappe complex and the overlying Tambo basement nappe (Gansser 1937; Strohbach 1965; Fig. 1) and represents the root zone of the Valaisan oceanic domain.

Sampling strategy

The most densely covered area lies between Lukmanier and Pizzo Molare in the west to Safiental in the east (see a complementary study on this area by Wiederkehr et al. 2008). Sampling is particularly dense between Olivone and Vrin (Fig. 2), where a pronounced lateral temperature gradient is indicated by the growth over an amazingly short distance (5 km along strike) of new porphyroblasts related to the Barrovian overprint (zoisite/clinozoisite, plagioclase, biotite and garnet).

In order to include additional samples located at considerable distance to the east and north from the closer area of investigation in Wiederkehr et al. (2008), and also to increase sample density, we also re-analysed reference samples used in previous studies (see Table 1). X-ray diffraction, combustion analysis, thermal analysis and vitrinite reflectance data (Petrova et al. 2002), as well as transmission electron microscopy (Ferreiro Mählmann et al. 2002) were previously presented along a profile that stretches from the part of the Misox Zone where amphibolite-facies conditions prevail (southernmost sample points in Fig. 1) all the way into the Prättigau half-window, which was only affected by very low- to low-grade metamorphism (in the northeastern corner of Fig. 1). These samples were reinvestigated in the present study not only in order to spatially extend the data set, but also for comparing these previous results with those obtained by Raman spectroscopy. Moreover, additional samples were taken from the collection of M. Frey (University of Basel) that were the subject of earlier investigations (Hoefs and Frey 1976; Frey 1978; Frey et al. 1982; Teutsch 1982; Thoenen 1989). The latter partly come from the Urseren-Garvera Zone (samples number 1–4 in Fig. 2 and Table 1) and somewhat increased the sample density in the adjacent Lukmanier area to the south and in the Misox Zone.

Raman spectroscopy of carbonaceous matter (RSCM method)

The continuous transformation of the crystalline structure of carbonaceous matter (CM) from disordered organic matter to fully ordered graphite (generally referred to as the graphitization process; e.g. Teichmüller 1987) is mainly temperature-dependent. Hence, the crystallinity of CM, referred to as degree of ordering (graphitization), is expected to increase systematically with increasing temperature and can therefore be used to estimate the metamorphic grade of a given rock sample (e.g. Quinn and Glass 1958; French 1964; Landis 1971; Grew 1974; Itaya 1981; Buseck and Huang 1985; Ferreiro Mählmann et al. 2002; Petrova et al. 2002). Numerous studies have shown that Raman spectroscopy is a reliable and powerful tool for recording the structural characterization (degree of ordering) of CM (e.g. Wang et al. 1989; Wopenka and Pasteris 1993; Beyssac et al. 2002b).

We monitor the regional changes in the structure of CM by using Micro-Raman spectroscopy. In contrast to other methods (X-ray powder diffraction, high-resolution transmission electron microscopy, isotope geochemistry or vitrinite reflectance measurements), Micro-Raman spectroscopy has the following advantages: (1) Raman spectra show significant changes with increasing metamorphic grade (e.g. Wopenka and Pasteris 1993; Beyssac et al. 2002b); (2) the method can be applied in a non-destructive way by in situ analysis and therefore permits the characterization of individual grains while preserving their petrological and textural relations; and (3) the sample heterogeneity can be quantified thanks to a high spatial resolution and short spectrum-acquisition time, which allows recording numerous spectra within a given sample. Hence, Micro-Raman spectroscopy of CM provides a precise indicator of metamorphic grade (Pasteris and Wopenka 1991; Yui et al. 1996), especially because the relationships between the degree of crystallinity as is expressed by the shape of the Raman spectra, and the metamorphic conditions have been calibrated as a geothermometer over a broad temperature interval from 330 to 650°C (Beyssac et al. 2002a). The calibration by Rahl et al. (2005) extended the range of the geothermometer to temperatures as low as 100°C and up to 700°C. (Rahl et al. 2005). A discussion of the calibration to lower temperatures is given in Lahfid et al. (2010).

Several studies showed that Raman spectroscopy of carbonaceous material (RSCM method) is the best-suited method for in situ determinations of the crystallinity of CM in thin sections (e.g. Pasteris and Wopenka 1991; Wopenka and Pasteris 1993; Yui et al. 1996; Beyssac et al. 2002b, 2003a). When empirically calibrated against independently determined temperatures (Beyssac et al. 2002a; Rahl et al. 2005), the spectra obtained provide a reliable geothermometer. It is important to note that the thermally induced graphitization process is strictly irreversible (e.g. Teichmüller 1987). Therefore, the structure of CM only depends on the maximum temperature reached along a given P–T-path and is insensitive to a polymetamorphic evolution and/or a retrograde overprint (Wopenka and Pasteris 1993; Beyssac et al. 2002a).

Because the 214 samples analysed for determinations of maximum temperature were collected in areas either dominated by subduction-related HP/LT metamorphism or dominated by collision-related MP/MT Barrovian overprint (Figs. 1, 2, Table 1), only the 3-D pattern of the temperatures derived by this method combined with additional petrological data allows one to discriminate between these

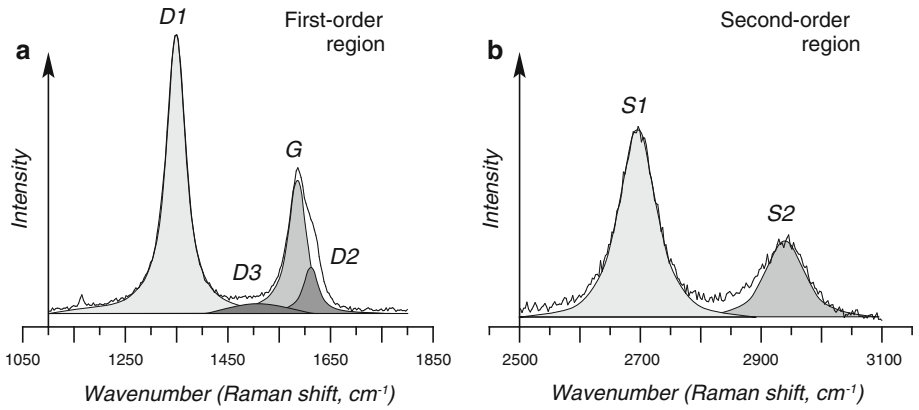

Fig. 3 Spectral deconvolution of the first- and second-order region of the Raman spectrum of CM, indicating a relatively disordered structure (sample Nr. 205 for which 350°C were inferred, see Table 1). **a** Position of the graphite G band and the D1, D2, D3 defect bands in the first-order region; **b** position of the graphite S1 and S2 bands in the second-order region

two events. All the results obtained by Micro-Raman spectroscopy were converted to peak-metamorphic temperatures by using both calibrations (Beyssac et al. 2002a; Rahl et al. 2005). In order to obtain comparable results, we strictly followed the analytical instructions given in Beyssac et al. (2002a, 2003b).

Sample preparation

The Raman spectra were recorded in situ, i.e. in conventionally polished petrographic thin sections, allowing for the preservation of the textural relationship between CM and the surrounding mineral matrix. Additionally, the surrounding rock matrix facilitates the removal of laser-induced heat, which may affect the degree of structural ordering due to the extreme sensitivity of CM to laser-induced heating during spectra acquisition (Beyssac et al. 2003b). Moreover, the recorded Raman spectra are highly sensitive to the orientation of CM due to its strong structural anisotropy, particularly in the case of well-crystallized graphite (e.g. Wang et al. 1989; Wopenka and Pasteris 1993). Recently, Tan et al. (2004) demonstrated that the Raman spectrum of mono-crystalline graphite is not very sensitive to polarization and orientation effects in the green part of the visible spectrum. However, we closely followed the instructions given in Beyssac et al. (2002a, 2003b) in order to avoid systematic variations. Therefore, the thin sections were cut perpendicular to the main foliation, and whenever possible, also parallel to the stretching lineation in order to record Raman spectra consistently in the same orientation, i.e. perpendicular to the expected mean stacking axis of the CM. In this way, it is possible to set the polarization of the laser beam perpendicular to the mean c-axis orientation of the CM.

Raman spectrum of carbonaceous material

In general, Raman spectra of CM can be decomposed into first-order (1,100–1,800 cm^{-1}) and second-order (2,500–3,100 cm^{-1}) regions (Tuinstra and Koenig 1970; Nemanich and Solin 1979; Fig. 3). The first-order region is perfectly suited for recording the degree of order/disorder of CM and thereby determining peak-metamorphic conditions (Pasteris and Wopenka 1991; Wopenka and Pasteris 1993; Yui et al. 1996; Beyssac et al. 2002a, b; Rantitsch et al. 2004; Rahl et al. 2005). This first-order region includes up to four Raman peaks or bands (Fig. 3a), including the G band characteristic of perfect crystallized graphite and up to three additional bands (generally called D1, D2 and D3) that are directly related to the degree of structural disorder (so-called defect bands; Tuinstra and Koenig 1970; Pasteris and Wopenka 1991; Beyssac et al. 2002a, 2003a; Nasdala et al. 2004).

The second-order region is mainly characterized by the appearance of two bands, S1 and S2 (Fig. 3b; Nemanich and Solin 1979; Wopenka and Pasteris 1993; Beyssac et al. 2003b; Lee 2004). As is the case regarding the first-order region, there are also systematic changes within the second-order region due to increasing graphitization (see e.g. Wopenka and Pasteris 1993; Beyssac et al. 2002a, b).

During progressive temperature-induced ordering, the Raman spectra of CM exhibit a characteristic evolution that is most obvious by looking at the intensities of bands related to disorder in the crystalline structure (D1, D2 & D3), but also evident from the position and width of the characteristic G band in the first-order region as well as from width and asymmetry of the S1 band in the second-order region (Pasteris and Wopenka 1991; Wopenka and Pasteris 1993; Yui et al. 1996; Beyssac et al. 2002a, b; Lee 2004). Beyssac et al. (2002a, b) showed that peak intensity ratio R1 (R1 = D1/G) and peak area ratio R2 (R2 = D1/[G + D1 + D2]), both calculated from bands in the first-order region, are the most reliable indicators for the degree of ordering in CM. They found a linear relationship between the R2 ratio and peak-metamorphic temperature in the range of 330–650°C by calibration with other geothermometers (Beyssac et al. 2002a). Recently, a revised calibration involving both R1 and R2 ratio was presented

by Rahl et al. (2005). The R1 ratio, taken into account by this second calibration method, shows significant variations, particularly under low- and very low-grade conditions. This contrasts with the R2 ratio, which is rather insensitive below 330°C and above 650°C (e.g. Beyssac et al. 2002a). Therefore, this revised calibration potentially extends the temperature range to the 100-700°C interval (Rahl et al. 2005). Due to uncertainties in the two calibration methods, the temperatures derived can only be accurate to within ±50°C (Beyssac et al. 2002a; Rahl et al. 2005). However, the precision is much better and allows inter-sample variations as small as ~10–15°C to be easily detected (Beyssac et al. 2004).

Analytical procedure: spectra acquisition and treatment

Micro-Raman spectroscopy was performed at the Raman Laboratory of the Institute of Earth and Environmental Sciences at Potsdam University using a confocal, notch filter-based spectrometer (LabRam HR 800, HORIBA Jobin–Yvon) equipped with an Olympus BX 41 microscope, an air-cooled Nd-YAG laser (Compass 315 M, Coherent) for Raman excitation with the 532 nm line and a Peltier-cooled CCD detector (Andor Technology). A Leica 50× microscope objective was used for sample viewing under both reflected and transmitted light, as well as for the Raman measurements. The laser spot diameter at the sample surface was about 3 μm, and the confocal pinhole was set to 200 μm. The laser power was reduced to 2–3 mW at the sample surface by a neutral D1 filter (transmission: 10% of the laser power) in order to exclude effects due to sample heating. The LabSpec software of HORIBA Jobin–Yvon has been used for data acquisition and estimation of the spectral parameters of the Raman bands. Before each session, a silicon standard was used for checking the calibration of the spectrometer. Since section preparation, particularly polishing, induces mechanical damage to the structure of CM (Nemanich and Solin 1979; Beyssac et al. 2003b), we focussed the laser beam onto CM matter located beneath a transparent mineral within the section (Pasteris 1989; Beyssac et al. 2002a, 2003b), preferentially beneath quartz, although calcite, feldspar and chloritoid were also used.

The application of a grating of 300 lines/mm and a slit width of 100 μm resulted in the acquisition of Raman spectra in the range 175–3,300 cm^{-1} with a spectral resolution of about 10 cm^{-1}. This configuration allowed for the registration of all first-order Raman bands of graphite in the region 1,100–1,800 cm^{-1} used for the estimation of the peak-metamorphic temperatures, and additionally the Raman bands of the covering transparent minerals, within a single spectral window. In each sample, a minimum of 10, and as many as 45 independent spots were analysed in order to gather insight regarding structural heterogeneities of the CM within one and the same sample. Depending on the intensity of the Raman bands, between two and four accumulations with an acquisition time ranging from 20 to 90 s were performed on each spot in order to improve signal to noise ratios of the spectra.

The Raman spectra were processed by using the program PEAKFIT 4.12 (Seasolve Software Inc.) with a Voigt function (combined Gaussian and Lorentzian profiles) and a linear background correction to determine the spectral parameters such as peak position, peak area, peak height and peak width FWHM (full width at half-maximum).

We used a 532-nm laser for Raman excitation instead of the 514-nm laser used in the calibration of Beyssac et al. (2002a). This is a crucial point due to the fact that the defect bands of CM exhibit a dispersive behaviour because it means that Raman band position and relative intensities vary with the excitation wavelength (Pocsik et al. 1998; Matthews et al. 1999; Cançado et al. 2006, 2007; Pimenta et al. 2007). Unfortunately, up to now there is no simple way to correct Raman parameters such as the R2 ratio for analyses performed by using the 532-nm laser. Being aware of the variations caused by a different laser wavelength, we are convinced that any systematic differences are of only minor importance for the following reasons (see also Aoya et al. 2010): (1) Numerous studies based on the calibration of Beyssac et al. (2002a) presented very reliable peak-metamorphic temperatures as obtained with the 532-nm laser in this study. These temperatures are generally in good agreement with the corresponding tectono-metamorphic setting (e.g. Rantitsch et al. 2004, 2005; Guedes et al. 2005; Judik et al. 2008; Kribek et al. 2008; Rantitsch and Judik 2009); (2) The geothermometer provided by Rahl et al. (2005) was calibrated with a 532-nm laser as well, and as discussed later (see "Comparison between the available calibration methods") and also shown by other investigations (e.g. Judik et al. 2008; Kribek et al. 2008), the recorded peak-metamorphic temperatures were generally close to those obtained by the calibration of Beyssac et al. (2002a); (3) Some samples investigated by this study were collected in the same area as that used for the calibration by Beyssac et al. (2002a; their sample "luk/Lukmanier"), i.e. from the area around Lukmanier (Fig. 1). The estimated R2 ratios for this area are in the range of 0.26–0.18 (Fig. 2, Table 1), i.e. well inside or close to the 0.24 ± 0.05 value determined for the R2 ratio by Beyssac et al. (2002a: sample "luk/Lukmanier" in their Table 2).

Results of the RSCM investigations

Table 1 summarizes the results of decomposing the spectra of all 214 samples and gives the estimated peak-metamorphic temperatures based on both calibrations (Beyssac et al. 2002a; Rahl et al. 2005) in terms of mean values. Measurement-induced uncertainties regarding the derived

temperatures are given as 95% confidence intervals (CI), i.e. close to 2σ errors corresponding to a confidence interval of 95.5%.

The change in metamorphic temperature over the entire area of investigation, ranging from lower/middle amphibolite-facies conditions in the southwest to lower greenschist-facies conditions with occasional blueschist-facies relics in the northeast (see Wiederkehr et al. 2008 for details), is directly illustrated by the corresponding evolution of the Raman spectra of CM, reflecting the degree of structural ordering as shown in Fig. 4. This evolution shows all the typical features described in earlier studies (e.g. Pasteris and Wopenka 1991; Wopenka and Pasteris 1993; Yui et al. 1996; Beyssac et al. 2002b) and will not be further discussed in this study.

Comparison between the available calibration methods

Given the exceptionally large number of measured samples and the large temperature interval covered in the study area, a comparison between the two available calibration methods by Beyssac et al. (2002a) and Rahl et al. (2005) is appropriate. Figure 5 graphically correlates the temperature estimates based on Beyssac et al. (2002a) with those obtained using Rahl et al. (2005). In general, the temperature differences between the two calibrations are well inside the ±50°C uncertainty inherent in the empirical calibration used by Beyssac et al. (2002a); both methods provide similar temperature estimates, discrepancies being less than 30°C (Fig. 5). At temperatures of 350, 425 and 530°C, both calibrations yield exactly the same temperature estimates. In the intermediate temperature intervals, some systematic differences are observed (Fig. 5). In the 450–525°C range, the temperatures calculated according to Rahl et al. (2005) are systematically lower, whereas the temperature estimates between 350–400°C and from 550°C upwards are higher than those calculated according to Beyssac et al. (2002a). The great advantage of the method of Rahl et al. (2005) is the possibility to estimate metamorphic temperatures in low- to very low-grade metasediments, i.e. in the 100–330°C temperature interval. In general, the relative uncertainties in temperatures derived with the calibration of Rahl et al. (2005) are higher, however, compared to those derived with Beyssac et al. 2002a, especially at temperatures higher than 480°C (see Table 1, Fig. 5).

Mapping thermal field gradients in 3 dimensions

Method used for contouring thermal field gradients in map and profile view

Based on the maximum temperatures obtained from the RSCM method, we present what we refer to as

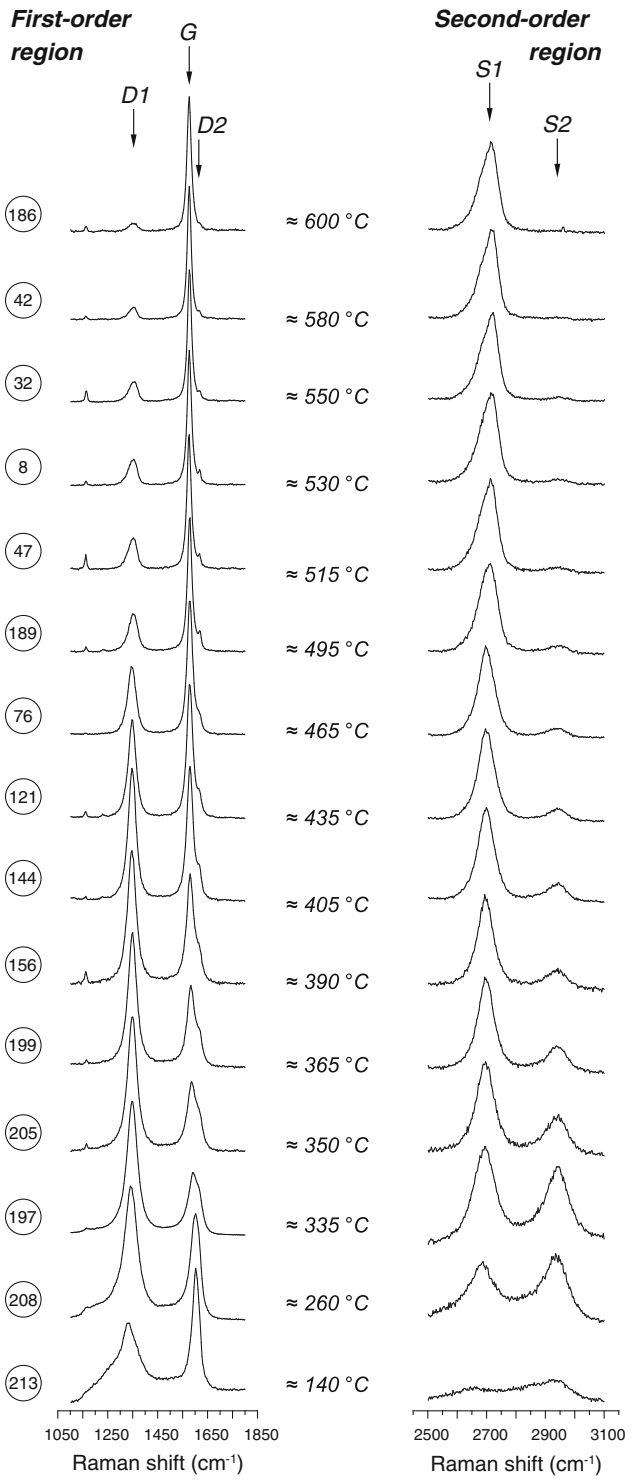

Fig. 4 Selection of representative first-order and corresponding second-order parts of the Raman spectra, arranged from bottom to top by increasing inferred temperatures and going from SW to NE across the area of investigation, respectively. The positions of the G, D1, D2, D3, S1 and S2 bands, as well as the estimated peak-metamorphic temperatures are indicated. The *numbers* on the *left-hand side* refer to the sample numbers listed in Table 1, for geographical locations see also Figs. 1, 2. The small narrow band at around 1,160 cm^{-1} in the first-order region is due to quartz as overlying transparent mineral; see text

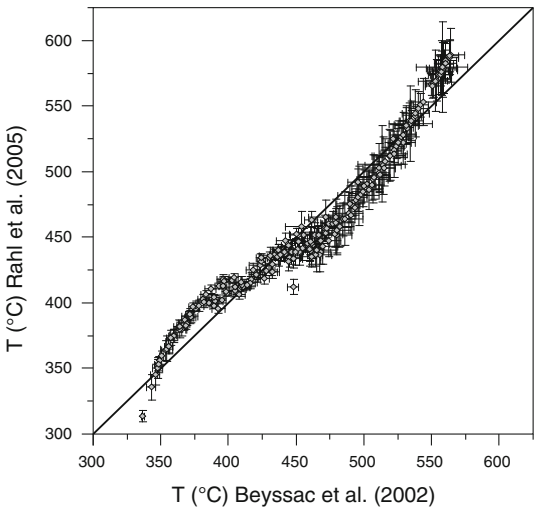

Fig. 5 Correlation of peak-metamorphic temperatures estimated based on the calibrations provided by Beyssac et al. (2002a) and Rahl et al. (2005), respectively, for all the analysed samples. See text for details

"isotemperature contours" in map and profile view. These contours simply represent lines connecting locations that reached a given maximum temperature in map or profile view, regardless of when these locations reached their maximum temperature and at which pressure. Note that these contours by no means necessarily represent true isotherms at a given instant in time, because maximum temperatures could have been reached at different times, as might indeed be expected given the complex metamorphic evolution of this area (see Wiederkehr et al. 2008, 2009 for details). Parts of the isotemperature contours reflect the temperatures reached during the earlier HP/LT event, or its subsequent greenschist-facies overprint during decompression, and are laterally continuous with other segments that record the temperatures reached during a later Barrow-type event.

When attempting to construct such contours, it soon became apparent that there is a rather small number of locations (16 locations out of a total of 214 measured) that obviously do not fit into a regional trend, neither in map nor in profile view, in that they exhibit much higher temperatures than their neighbouring specimens. These are highlighted with bold letters in Table 1 and were not included in the construction of the isotemperature contours. Dealing with such discrepancies that can be attributed to the heterogeneous nature of natural carbonaceous matter (e.g. Beyssac et al. 2002b; Aoya et al. 2010) is a challenge when using the RSCM method (e.g. Beyssac et al. 2003b).

Four reasons are held responsible for such discrepancies: First, such heterogeneities may be caused by depositional mixing of sedimentary detritus (e.g. Diessel et al. 1978; Itaya 1981; Petrova et al. 2002). Thus, one can obtain peak temperatures valid for the source area rather than for the metasediments sampled. A recent study performed along the metamorphic profile from the Prättigau half-window to the Misox Zone (Fig. 1) provided evidence for the common occurrence of detrital graphite in nearly all samples, as documented by X-ray diffraction data (Petrova et al. 2002). The widespread occurrence of detrital graphite is in agreement with the study by Galy et al. (2008) addressing recycling of graphite.

Secondly, such discrepancies may reflect the fact that the metamorphic structure of the Central Alps is rather complex. The occurrence of closely juxtaposed tectonic units with drastically different peak-metamorphic conditions is a common feature. Hence, inter-sample heterogeneities may simply reflect variations in the tectono-metamorphic evolution of different tectonic units.

Thirdly, such heterogeneities may be caused by the fact that the graphitization process is not strictly temperature-dependent. Reasons for this include the effects of pressure (Diessel et al. 1978; Teichmüller 1987), tectonic stress/strain (Bustin et al. 1986; Suchy et al. 1997; Ferreiro Mählmann et al. 2002; Nover et al. 2005; Aoya et al. 2010), duration of the thermal/metamorphic event (e.g. Itaya 1981; Okuyama-Kusunose and Itaya 1987), host-rock lithology (e.g. Grew 1974; Wopenka and Pasteris 1993; Wada et al. 1994), catalytic species/minerals (e.g. Bonijoly et al. 1982; Okuyama-Kusunose and Itaya 1987 and references therein), type of organic precursors (Kribek et al. 1994; Large et al. 1994; Bustin et al. 1995) and composition/activity of metamorphic fluids (Large et al. 1994; Guedes et al. 2005).

Finally, the entire analytical procedure may induce heterogeneities due to the measurement technique itself or due to the fitting procedure (e.g. Beyssac et al. 2003b). In order to minimize such effects, we closely followed the instructions given by Beyssac et al. (2002a, 2003b) thereby avoiding systematic inter-sample variations.

A detailed discussion of the samples yielding abnormally high temperatures in respect to neighbouring specimens (highlighted in bold letters in Table 1) will be provided in the Interpretation/Discussion paragraph.

The isotemperature contours were drawn manually based on the calibrations of Beyssac et al. (2002a) and Rahl et al. (2005) in Fig. 6, and based on Beyssac et al. (2002a) in Figs. 7 and 8. We contoured the data manually, because we also tried to keep the spacing between isolines more or less constant, had to exclude some of the specimens (see below) and, in case of the Lunschania antiform, also used structural information. The resulting manually constructed peak-temperature contours were found to be close to those obtained by geostatistical methods using a kriging routine.

In the temperature–distance and temperature–altitude profiles presented in Figs. 7 and 8, respectively, and prior to the contouring within the plane of the section, the

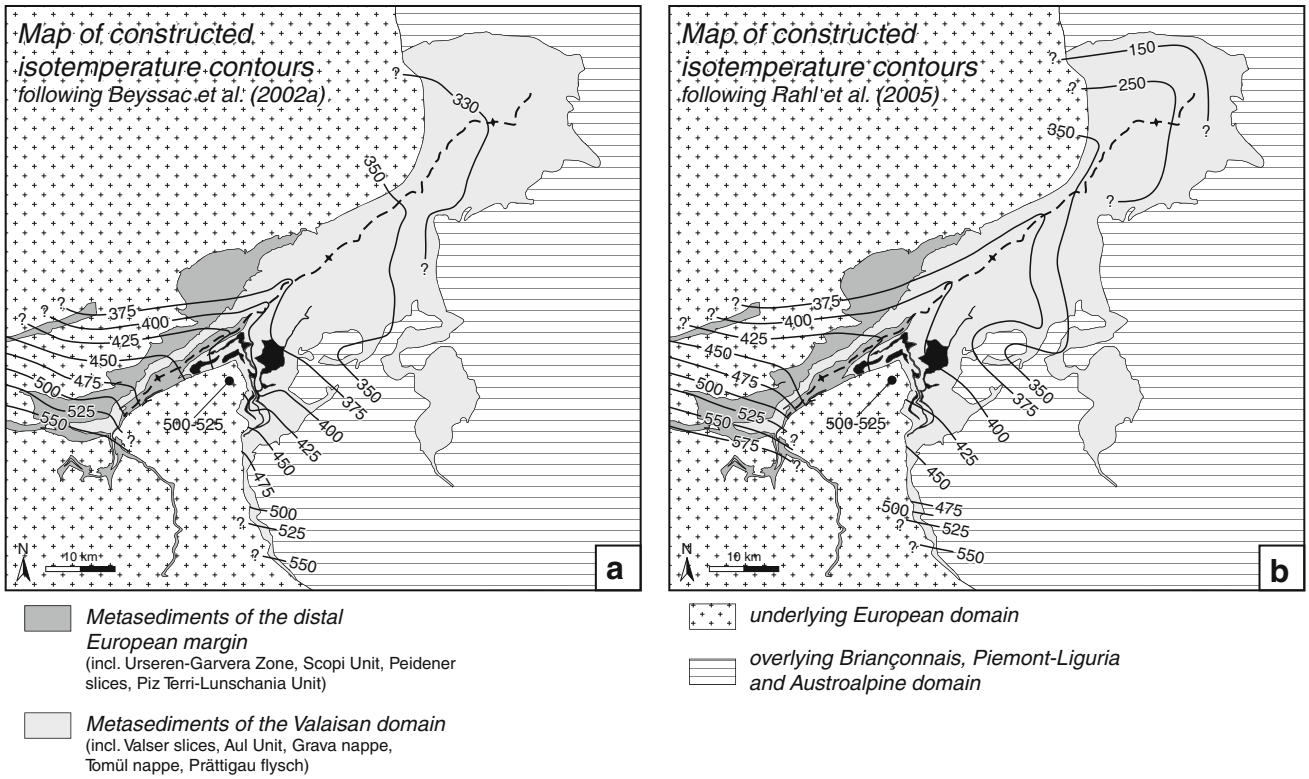

Fig. 6 Comparison of the estimated peak-metamorphic temperature distribution in map view in the form of isotemperature contours (see text) derived from the samples listed in Table 1 using the calibrations given by **a** Beyssac et al. (2002a), and **b** Rahl et al. (2005). Temperatures are given in °C. *Stippled line* indicates the trace of the axial plane of the Lunschania antiform

sample locations were projected into the profile plane in a direction parallel to the isotemperature contours, as previously constructed in map view (Fig. 6) and from within a corridor whose width is given in the figure captions. The sample localities were projected horizontally in the case of Figs. 7 and 8a, and by using the angle of the local axial plunge specified in the figure caption in case of Fig. 8b–e.

Comparison of the thermal field gradients obtained with two alternative calibration methods

We first present the peak-metamorphic temperatures obtained by the RSCM method as a function of geographical location (see also Table 1). The two maps depicted in Fig. 6 based on the two available calibrations predict comparable and very reliable peak-metamorphic temperatures that vary from <330°C in the northeast (Prättigau half-window) up to 560–590°C in the southwest (Pizzo Molare, Lepontine thermal dome; Table 1, Fig. 6).

Both maps show similar shapes of the constructed isotemperature contours, especially for the 425 and 525°C range (compare Fig. 6a, b). It is also remarkable that in both maps the 375, 400 and 425°C isotemperature contours show the same characteristic curved indentation towards the northeast in map view. As discussed in Wiederkehr et al. (2008), this feature is related to the fact that the isotemperature contours in the northeast record temperatures that were acquired during the earlier metamorphic evolution and were subsequently folded around a NE-plunging antiform (Lunschania antiform of Voll 1976). However, this excursion towards the northeast is not shown by the isotemperature contours in the 450–550°C range that are aligned more or less parallel to a NW–SE-direction, i.e. perpendicular to the predominant metamorphic field gradient in the western part of the investigated area. There, these isotemperature contours are related to temperatures that prevailed during the Barrow-type event and that were higher than those acquired during the earlier HP/LT stage and/or subsequent greenschist-facies overprint. This Barrow-type event not only post-dates an earlier HP/LT stage, but also the subsequent folding of the older field temperature gradient (e.g. Wiederkehr et al. 2008).

The most obvious discrepancies between Fig. 6a and b, i.e. between the field temperature gradients derived from the two alternative calibrations, are found in the northeast, i.e. at low temperatures. The temperature distribution

pattern of the Rahl et al. (2005) (Fig. 6b) calibration generally shows a higher maximum temperature gradient, as revealed by additional isotemperature contours down to 150°C. This independently illustrates the advantages of using the Rahl et al. (2005) calibration at low temperatures. Minor discrepancies are also found in two other areas: In the intermediate temperature domain above about 450°C, the isotemperature contours derived from the Rahl et al. (2005) calibration appear more closely spaced, which reflects a higher temperature gradient. In particular, the 450°C isotherm is shifted to the west. Moreover, in the highest-temperature domain slightly higher temperatures are inferred and an additional isotemperature contour at 575°C had to be constructed when analysing the temperatures obtained from the calibration of Rahl et al. (2005).

We conclude that despite minor discrepancies, both calibrations yield essentially identical features at temperatures higher than 330°C, features that are mainly characterized by a field temperature gradient that decreases radially away from the Lepontine dome in the southwest towards the Prättigau half-window in the northeast, superimposed on an excursion of the isotemperature contours to the northeast that coincides with an antiform which folds isotemperature contours lower than about 450°C. In the following, we present the peak-metamorphic temperatures obtained in more detail, as well as thermal field gradients in profile view, thereby addressing the third dimension of the spatial distribution of maximum temperatures.

Peak temperatures along the Pizzo Molare-Domleschg profile

Along this SW–NE-oriented profile (Fig. 7a) metasedimentary units derived from both the European margin and the Valais oceanic domain are exposed continuously. This allows a clear correlation of deformational phases and relative timing of metamorphic events along strike (Wiederkehr et al. 2008). These authors showed that both the metasediments of the Valaisan domain (Grava nappe) and parts derived from the distal European margin (Peidener slices) are characterized by a bimodal P–T-path in which the amphibolite-facies Barrovian overprint represents a distinct heating pulse that followed isothermal or nearly isothermal decompression from an earlier HP/LT blueschist-facies event. Hence, most of the specimens analysed derive from this profile in which temperature ranged from 560–590°C in the southwest down to 350–370°C in the northeast (Fig. 7a).

The highest temperatures were obtained at localities near Pizzo Molare and Grumo (northern Valle di Blenio; Fig. 1), which marks the northeastern edge of the high-temperature part of the Lepontine thermal dome characterized by amphibolite-facies, Barrow-type metamorphism (e.g. Engi et al. 1995; Todd and Engi 1997; Frey and Ferreiro Mählmann 1999) and where recorded temperatures decrease radially towards the north and northeast. The overall thermal field gradient along this SW–NE section partly exhibits a relatively high lateral thermal field gradient along Val Luzzone, ranging from 540°C north of Olivone down to 430–450°C around the Piz Terri over a distance of only 10 km (Fig. 7a). This portion with a high lateral gradient coincides with dramatic changes in the mineralogy of the metasediments (Wiederkehr et al. 2008) and is interpreted to represent the northeastern edge of the Lepontine Barrow-type thermal dome. Further to the northeast, between Vrin and Safiental/Domleschg (Fig. 7a), the lateral thermal field gradient is significantly lower, within the 450–350°C interval (Fig. 7a).

Interestingly, this change in the lateral thermal field gradient also coincides with a change in the inclination of the isotemperature contours in Fig. 8a. This figure enables a reliable construction of the steepness of the isotemperature contours in a region of high relief and dense sampling. Across Val Luzzone, the isotemperature contours steepen to some 30–45° inclined to the northeast, but flatten towards the east in the area of Piz Terri (Fig. 8a). The metamorphic field gradient (not necessarily equal to a geothermal gradient) amounts to some 14°C/km. Further, the change to a more moderate inclination northeast of Piz Terri (Fig. 8a) coincides with a significant change in the trend of the isotemperature contours in map view, as discussed earlier: in the southwest (i.e. where the contours are steeply inclined in Fig. 8a) they cut across the Lunschania antiform, whereas further to the northeast they are folded by this same antiform (Fig. 6). This supports the interpretation that the isotemperature contours reflect the maximum temperatures reached during at least two separate metamorphic events that pre-date and post-date folding of the Lunschania antiform, respectively.

Peak temperatures along two profiles across folded isotemperature contours

Effects due to the folding of the Tmax-contours (Wiederkehr et al. 2008) are visualized by two temperature–distance profiles oriented at a high angle to the fold axis of the Lunschania antiform depicted in Fig. 7b (Splügen-Ilanz) and Fig. 7c (Misox Zone-Ilanz). Both profiles show a localized temperature peak reaching some 425°C in the Valsertal and coinciding with the core of the Lunschania antiform, superimposed onto the overall lateral thermal field gradient. This corroborates the idea of folded isotemperature contours in the eastern part of the working area. Interestingly, the transition between folded and intersecting isotherms is located between 450 and 425°C

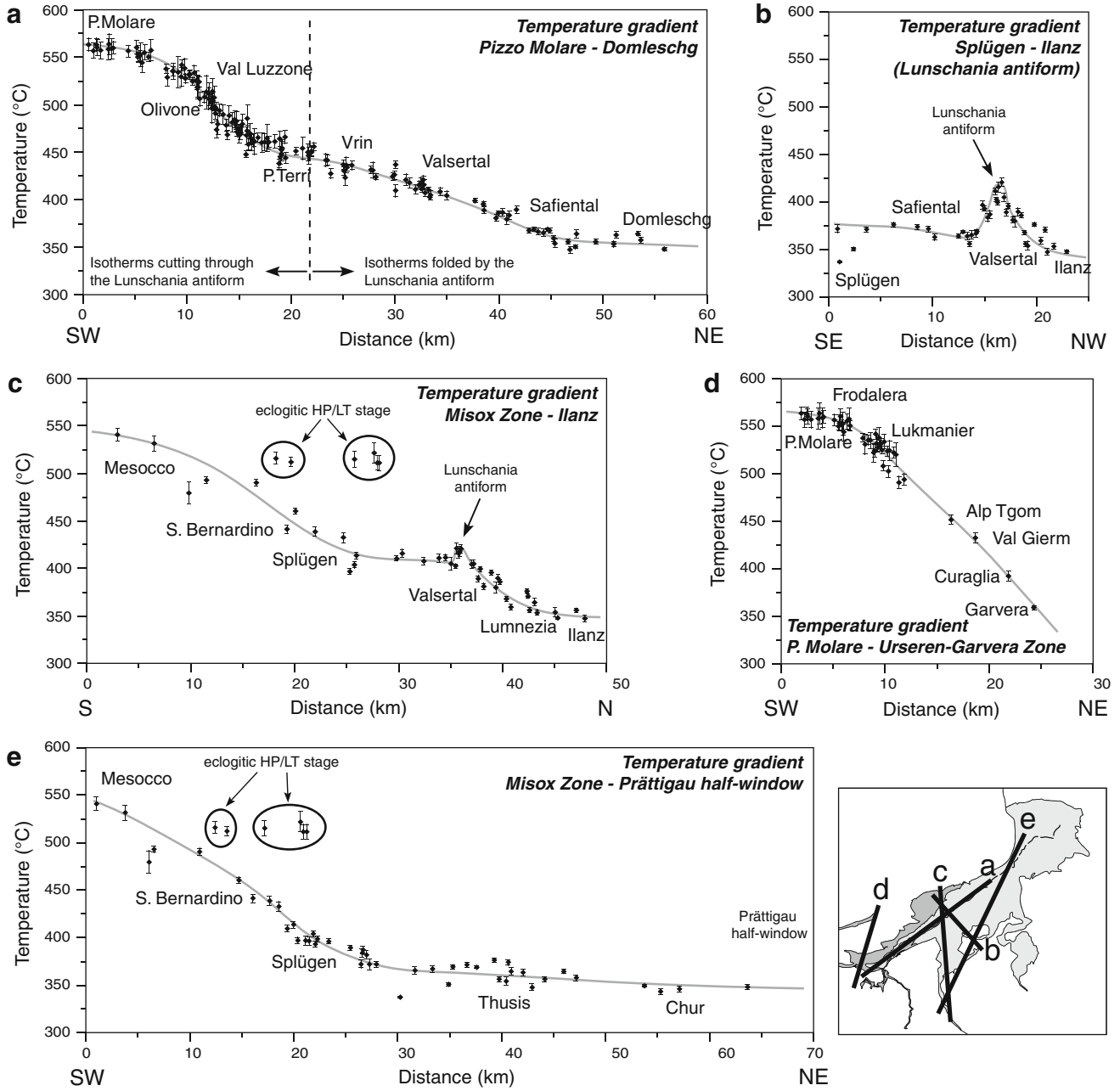

Fig. 7 Temperature–distance profiles summarizing the peak-metamorphic temperatures as inferred by the RSCM method using the Beyssac et al. (2002a) calibration method along NE–SW to N–S trending profile traces, whose locations are indicated in an inset (*lower right*). The samples and inferred temperatures listed in Table 1 were projected into the cross-section plane perpendicular to the isotemperature contours shown in Fig. 6a from within a corridor of the following width: **a** 16 km for profile P. Molare—Domleschg; **b** 6 km for profile Ilanz—Splügen; **c** 10 km for profile Misox Zone—Ilanz; **d** 10 km to the WNW and 7 km to the ESE off the profile trace for profile P. Molare—Urseren-Garvera Zone; **e** 20 km for profile Misox Zone—Prättigau half-window. *Line* represents manual best of the temperature–distance gradient. *Encircled samples* are from specimens that record temperatures related to an upper blueschist/eclogitic HP/LT stage (see text for "Discussion"). See Fig. 1 for the location of geographic localities

(see Fig. 6). This is within the temperature interval where the steep lateral thermal field gradient becomes flatter towards the east (Figs. 7a, 8a). All this clearly indicates that the isotemperature contours record the older HP/LT metamorphic event and/or immediately subsequent greenschist-facies overprint in the northeast, whereas in the southwest they record the younger Barrow-type event, where obviously the temperatures associated with the older

HP/LT event were reset during Barrow-type thermal overprinting.

Peak temperatures along the Pizzo Molare-Urseren-Garvera Zone profile

Owing to the lack of metasediments on the basement of the Gotthard unit, maximum temperatures along this profile (Fig. 7d) are rather poorly constrained in its northern part, where only four samples (samples 1–4, Table 1; Fig. 2) from a thin veneer of Mesozoic sediments from the E–W striking Urseren-Garvera Zone were suitable for analysis. Nevertheless, this profile provides important information concerning the northern limit of the Lepontine thermal dome in an area that experienced no prior HP/LT overprint (Urseren-Garvera Zone and Scopi Unit). Hence, the Tmax field gradient is expected to be solely related to the late-stage Barrow-type event. This is corroborated by the thermal field gradient in Fig. 7d, characterized by a continuous temperature decrease from 560–590°C at Pizzo Molare to 450°C at Alp Tgom (sample 1) and finally to 360–375°C at Garvera (sample 4). A high lateral thermal field gradient is also reflected in the close spacing of the isotemperature contours in Fig. 6; a similarly high gradient is recorded along Val Luzzone (Fig. 7a).

Peak temperatures along the Misox Zone-Prättigau profile

The transition from subduction-related HP/LT metamorphism and associated subsequent greenschist-facies overprint to collision-related, Barrow-type metamorphism is also preserved along this profile (Fig. 7e). Also shown are the data from the frontal part of the Adula nappe complex ("internal Mesozoic", Löw 1987) and from the adjacent northern Misox Zone (Aul Unit), characterized by much higher peak-metamorphic temperatures. These units experienced an upper blueschist/eclogitic HP/LT event during which considerably higher temperatures were reached than in the surrounding carpholite-bearing metasediments, i.e. Grava and Tomül nappes (see presentation of the Adula nappe complex below).

Due to the significantly lower density of investigated samples, only a rough overview of this profile can be given. Peak-metamorphic temperatures range from 540–550°C in the southern Misox Zone down to 130–140°C in the northeastern part of the Prättigau half-window (Fig. 6b). The overall trend of decreasing temperatures towards the north is again not uniform. Whereas a remarkable lateral thermal field gradient between Mesocco and Splügen is marked by a rapid decrease in temperatures from 540–550°C down to 370–390°C, the maximum temperatures stay remarkably constant in the 350–375°C range (Fig. 7e) further to the northeast.

A closer look at the Misox Zone reveals a more complex pattern: Samples 190 and 191 (Table 1) taken from the boundary area with the Adula nappe complex as well as samples 146–149 (Table 1) collected inside the northern Adula nappe complex indicate locally higher maximum temperatures in the range of 500–515°C. This is not in accordance with the overall south-to-north trend of decreasing peak-metamorphic temperatures ("eclogitic HP/LT event" indicated in Fig. 7c, e). These anomalously high temperatures were obtained from Grt-Ctd micaschists in the southern continuation of the Aul Unit (Gansser 1937; Steinmann 1994) as well as from Ky-Grt-Ctd-Zo micaschists of the internal Mesozoic sediments of the Adula nappe complex (see further explanations for the Adula below).

Peak-metamorphic temperatures obtained for the northern Adula nappe complex

Only four samples (Ky-Grt-Ctd-Zo micaschists) from the frontal part of the Adula nappe complex were suitable for analysis (samples 146–149). The peak-metamorphic temperatures all cluster around 500–520°C. In the surrounding metasediments, maximum temperatures are estimated at 410–430°C. This clearly indicates a jump in peak-metamorphic conditions of some 100°C across the nappe boundary (Fig. 6). This jump clearly indicates that the Adula nappe complex had a different metamorphic evolution than that of the surrounding metasediments (except for the localities of samples 190 and 191 mentioned above).

Peak temperatures projected onto a series of N–S-oriented tectonic cross-sections

In order to better illustrate the three-dimensionality of the pattern of peak temperatures and the spatial relationships between isotemperature contours and tectonic units, the inferred maximum temperatures were projected along strike into a series of N–S-oriented tectonic cross-sections (Fig. 8b–e; see Wiederkehr et al. 2008 for a description of additional structural details revealed in these four cross-sections). Using the measured axial plunge of the structures and assuming cylindricity of the structures, the profiles are arranged so as to reveal the large-scale structure of the area. Note, however, that the isotemperature contours run across strike (see Fig. 6) and are therefore discordant to these approximately cylindrical structures along strike. For this reason, they should not be connected from one profile to the next perpendicular to strike. Hence, the contours are only valid for the individual profile for which they are drawn. It is also important to emphasize that the isotemperature contours in Fig. 8b–e are by far less well constrained than along strike as depicted in Fig. 8a. This is because Fig. 8a is based on a much higher density of data.

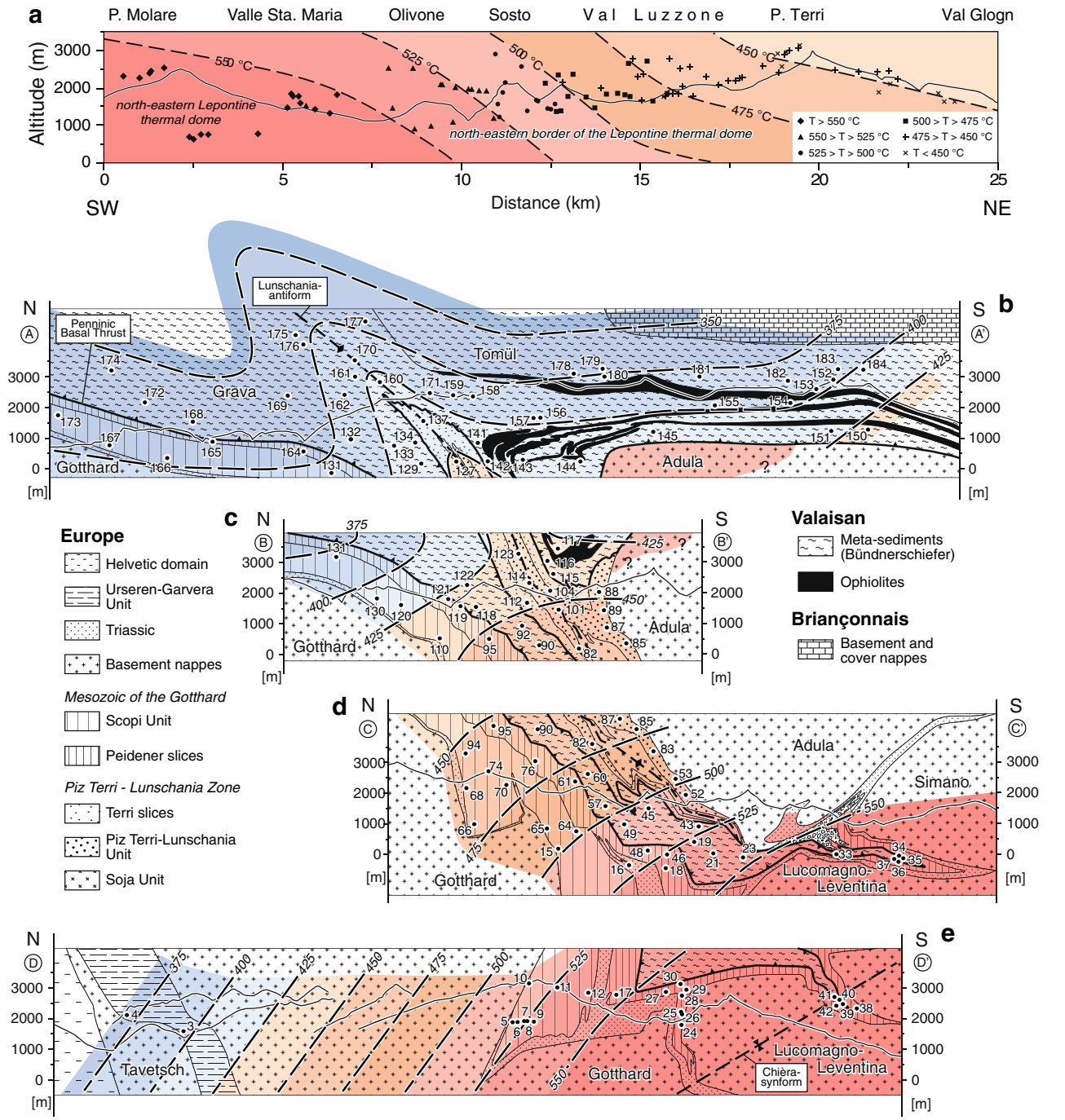

Fig. 8 Temperature-altitude cross-sections through the northeastern rim of the Lepontine thermal dome and easterly adjacent areas. The trace of cross-section **a** is the same than for profile shown in Fig. 7a (see inset in Fig. 7 for location), traces of these cross-sections **b–e** are indicated in Fig. 2; the across strike sections (Fig. 8b–e) show the main structural features (after Wiederkehr et al. 2008) for comparison. Peak-metamorphic temperatures inferred by the RSCM method are displayed in the form of isotemperature contours (see text) derived from the samples listed in Table 1 using the calibrations given by Beyssac et al. (2002a). The slopes of the isotherms were estimated within the plane of the cross-section after projecting the sample locations and associated peak-metamorphic into the cross-section plane. **a** Along-strike profile with samples horizontally projected from within a 14-km-wide corridor and parallel to the constructed peak-metamorphic isolines shown in Fig. 6. In case of the across strike profiles (see Wiederkehr et al. 2008 regarding structural details), width of the corridor from within which specimens were projected, and projection procedures are as follows: **b** 14-km-wide corridor, projection towards east and west by using local azimuth and plunge of the Lunschania antiform (060/12) for the northern part and a plunge of 20° to the east for the southern part of the cross-section; **c** 12-km-wide corridor, projection towards the east and west by using local azimuth and plunge of the Lunschania antiform (064/16); **d** corridor limited by 2.5 km to the E and some 6 km to the W of the profile trace, projection towards the east and west by using local azimuth and plunge of Chièra phase-related fold axes (090/30); **e** 12-km-wide corridor, projection towards the east and west by using local azimuth and plunge of Chièra phase-related folds axes (090/20)

Nevertheless, and despite considerable uncertainties regarding slope and position of the isotemperature contours in Fig. 8b–e, the following salient features can be confidently extracted from these cross-sections: (1) The inclination of the isotemperature contours flattens in the southern parts of Fig. 8c–e, but steepen in the northern portions of the same cross-sections. This reflects the fact that the Barrovian overprint (Lepontine thermal dome) that determines the maximum temperatures in the northern part of these sections also cuts across structures in a N–S direction and not only across strike of these structures as seen in map view (Fig. 6); (2) In contrast to the cross-sections located further to the west (Fig. 8c–e) that are generally characterized by steeply N-dipping isotherms, the easternmost cross-section exhibits a more complex pattern with isotherms folded around the Lunschania antiform (Fig. 8b). This supports the aforementioned inferences for Fig. 7b, c that it is the older pre-Lunschania antiform LT regime (blueschist-facies metamorphism and/or subsequent greenschist-facies overprint) that is recorded by the maximum temperatures in the eastern part of the working area, whereas the isotemperature contours related to the late-stage Barrow-type metamorphic event cut across this antiform. This independently confirms inferences made by Wiederkehr et al. (2008) based on structural and other petrological criteria.

Discussion

Comparison between RSCM-derived maximum temperatures and temperatures inferred from other petrological data

Figure 9 compares the RSCM-derived temperatures with those expected from the occurrences of index minerals, and/or from the P–T-paths. These paths are inferred from the analysis of mineral parageneses and thermodynamic modelling of equilibrium phase diagrams (e.g. Wiederkehr et al. 2008; Wiederkehr 2009). In the following, we discuss the presented maximum temperatures and compare them with temperature estimations inferred from other petrological data for the different tectono-metamorphic domains.

HP/LT units of the Valaisan and the adjacent Europe-derived domains

Occurrences of Fe–Mg carpholite, the diagnostic HP-mineral found in metasediments of the Valaisan domain and parts of the metasediments derived from the distal European margin (Goffé and Oberhänsli 1992; Oberhänsli et al. 1995; Bousquet et al. 2002, 2008; Wiederkehr et al. 2008), document the HP/LT blueschist-facies event in the eastern part of the working area. West of this LT area, relics of carpholite are found all the way up to the 500°C isotemperature contour. Pseudomorphs after carpholite were even found in the vicinity of Pizzo Molare, i.e. up to >550°C (Fig. 9). This clearly documents that this western area formerly was also part of a through-going blueschist-facies metamorphic belt that stretched from the Engadine window all the way to the Western Alps (Bousquet et al. 2002, 2008). Glaucophane (Gansser 1937; Nabholz 1945; Oberhänsli 1977, 1978) and jadeite (Santini 1992; Ring 1992) are the other minerals that are diagnostic for this earlier subduction-related blueschist-facies event. Within the low-grade Fe–Mg carpholite-bearing metasediments, chloritoid only rarely occurs within the Fe–Mg carpholite-bearing quartz-calcite veins/segregations. In such cases, chloritoid is interpreted as a part of the HP/LT assemblage (see also "Discussion" by Oberhänsli et al. 2003). However, most of the chloritoid found in the area formed during the late-stage greenschist-facies overprint rather than during the high-pressure event (Rahn et al. 2002; Wiederkehr 2009). This is supported by the observation that chloritoid generally occurs as idiomorphic rosettes, bundles and prisms (e.g. Wiederkehr et al. 2008). Based on the mineral chemistry of the observed mineral assemblage, peak-metamorphic conditions of 1.2–1.4 GPa and 350–400°C were estimated for the blueschist-facies stage in metasediments of the Grava and Tomül nappes, as well as in some of the metasediments derived from the European margin (Peiden slices and Piz Terri-Lunschania Unit; Wiederkehr et al. 2008).

For areas not affected by the subsequent Barrow-type metamorphic event, the isothermal or near-isothermal decompression of the Valais Ocean-derived Bündnerschiefer and the Europe-derived Peidener Schuppenzone occurred after the HP blueschist-facies stage (see P–T-paths indicated in Fig. 9, based on the studies of Bousquet et al. 2002 and Wiederkehr et al. 2008). This is supported by Rahn et al. (2002) inference of 400 ± 50°C for greenschist-facies metamorphism of the Tomül nappe, based on chloritoid-chlorite and chlorite thermometry. This may be taken to show that the Barrow-type overprint never affected the eastern areas depicted in Fig. 9. Alternatively, such an overprint may have been associated with temperatures less than 400°C, i.e. less than the temperature range previously reached during the blueschist-facies event and/or during the subsequent isothermal decompression. Because folding leading to the Lunschania antiform took place after the decompression from the blueschist-facies conditions, the isotemperature contours at or below 400°C are expected to appear folded by this antiform, as indicated by our data (Figs. 7, 8). Folded isotemperature contours are also indicated by Weh (1998) and Petrova et al. (2002). These authors report a metamorphic high around Chur (Fig. 1)

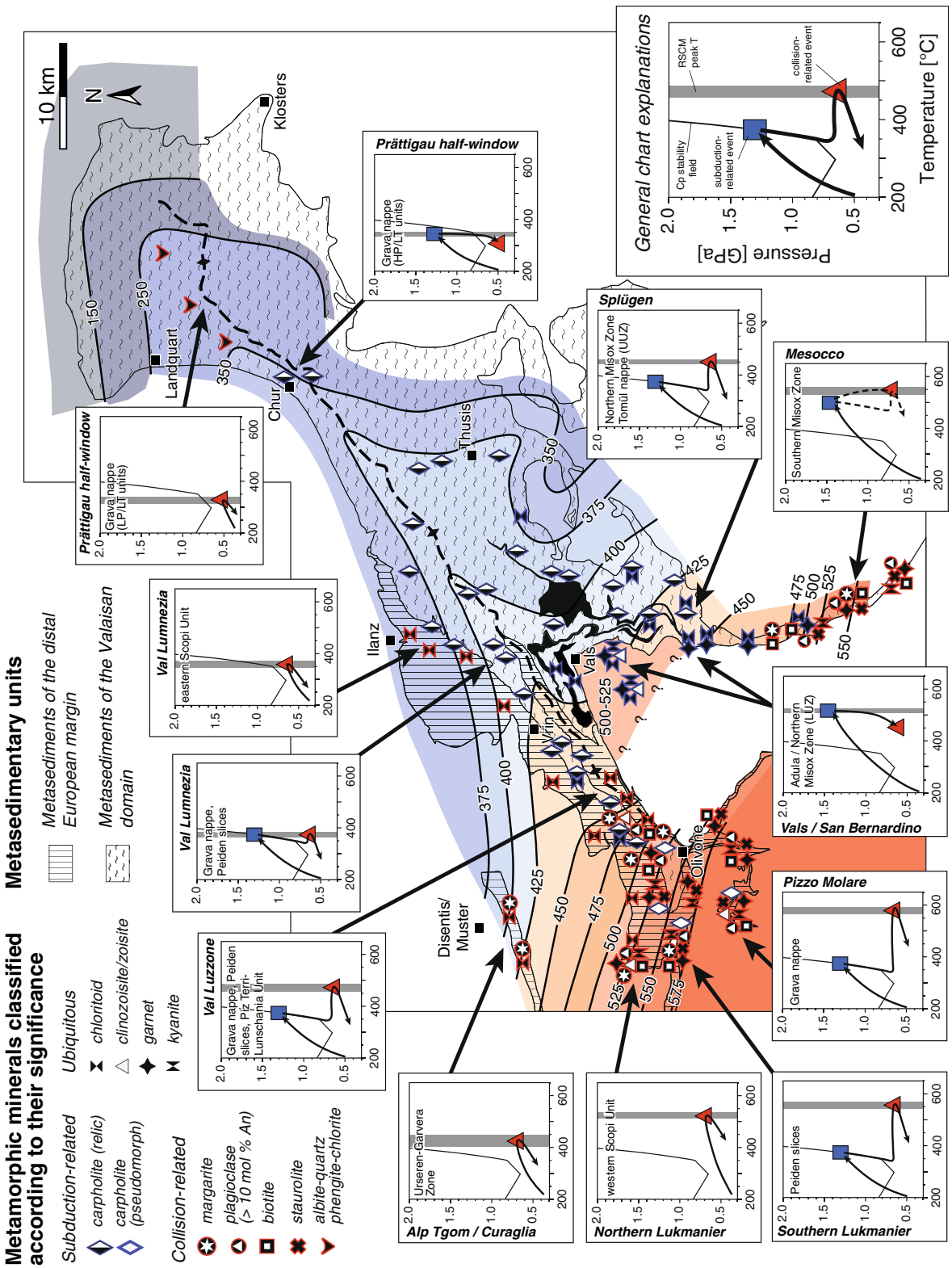

Fig. 9 Map providing a comparison between RSCM-derived temperatures (isotemperature contours of Fig. 6b and occurrences of index minerals, as well as selected P–T-paths derived from mineral parageneses and thermodynamic modelling of equilibrium phase diagrams (Wiederkehr et al. 2008; Wiederkehr 2009) and literature data (Frey 1974; Frey et al. 1982; Teutsch 1982; Heinrich 1982, 1986; Löw 1987; Santini 1992; Ring 1992; Frey and Ferreiro Mählmann 1999; Ferreiro Mählmann et al. 2002 and references therein; Bousquet et al. 2002 and references therein). *Inset* General chart explanations; *LUZ* Lower Uccello Zone (corresponding to Aul Unit; Steinmann 1994); *UUZ* Upper Uccello Zone (corresponding to Tomül nappe; Steinmann 1994)

that is located in the core of the Lunschania antiform and was interpreted to have formed by post-metamorphic deformation. These older findings are confirmed by our study (Figs. 7, 8) that also demonstrates the high spatial resolution of the maximum temperature pattern obtained with the RSCM method and a dense sampling network. In summary, the RSCM-derived peak-metamorphic temperatures are in excellent agreement with other available T-estimates (350–400°C; Bousquet et al. 2002; Rahn et al. 2002). However, an unambiguous attribution of the temperature estimates to a specific early stage of the P–T-evolution, i.e. either to peak pressures during HP-metamorphism or to subsequent greenschist-facies decompression, is not possible.

Prättigau half-window

Metamorphic grade that increases from diagenesis to lower greenschist grade conditions in the eastern Prättigau half-window to greenschist-facies conditions further to the southwest was also described in previous work (e.g. Frey and Ferreiro Mählmann 1999; Ferreiro Mählmann et al. 2002; Petrova et al. 2002). Hence, the temperature pattern derived by the RSCM method appears to be reliable also at low temperatures, particularly when using the Rahl et al. (2005) calibration method (Fig. 6b).

Northeastern Lepontine thermal dome

An increase in metamorphic grade is also established in a N–S direction and across Europe-derived metasediments in the northwestern part of the working area (Fig. 9), i.e. across northerly areas that never experienced blueschist-facies overprint. The peak temperatures obtained by the RSCM method for the Urseren-Garvera Zone range from 360–450°C (Table 1) and hence are in excellent agreement with chlorite-chloritoid and calcite-dolomite thermometers that yield 390–510 and 360–480°C, respectively (Livi et al. 2002), as well as with temperature estimates of 400 ± 50°C based on chlorite-chloritoid and chlorite thermometry (Rahn et al. 2002). Based on the investigation of the isotopic composition of carbonaceous matter, Hoefs and Frey (1976) presented strongly scattered, considerably lower metamorphic temperatures ranging from 250°C in the Urseren-Garvera Zone to 750°C in the Lukmanier area. They claimed equilibrium exchange reactions and kinetic isotopic effects, i.e. oxidation in the presence of water, to be responsible for this scatter. The progressive southward increase in metamorphic grade up to lower/middle amphibolite-facies conditions in the Lukmanier and Pizzo Molare area was established early on (Chadwick 1968; Frey 1969, 1974, 1978; Thakur 1971; Fox 1975). Staurolite-kyanite-garnet-bearing micaschists indicate lower to middle amphibolite-facies peak-metamorphic conditions at 0.5–0.8 GPa and 500–550°C (Chadwick 1968; Engi et al. 1995; Todd and Engi 1997; Frey and Ferreiro Mählmann 1999). Interestingly, Fox (1975) made an early attempt to discern the three-dimensional pattern of the metamorphic zonation based on isograds obtained from isochemical Jurassic black shales. In the area around Lukmanier, he estimated a minimum dip of these isograds of 35° towards the north, which is in agreement with the dip of our isotemperature contours (40–55°; Fig. 8e). Recently published data obtained along a N–S metamorphic transect predict 0.6–0.8 GPa at 530–575°C for the Lukmanier area in the north, 0.6 GPa at 550°C in an intermediate area (northern Valle di Blenio) and finally 0.7–0.85 GPa at 580–600°C for Pizzo Molare in the south (Janots et al. 2008). In summary, the predicted peak-metamorphic temperatures determined by the RSCM method are in good agreement with observed mineral assemblages, also in this part of the working area.

Northern Adula nappe complex and Misox Zone

As discussed earlier, the frontal part of the Adula nappe complex experienced an upper blueschist/eclogitic overprint (Löw 1987; Heinrich 1986; Zulbati 2008), in contrast to the surrounding high-pressure terranes that experienced blueschist-facies metamorphism at considerably lower temperatures, as documented by occurrences of Fe–Mg carpholite. Here too, the RSCM-derived temperatures are in perfect agreement with the temperatures inferred for this upper blueschist/eclogite-facies event. Petrological investigations on eclogites and metapelites yield temperature estimates related to high-pressure metamorphism of the northern Adula nappe that are consistent with our estimates: 470–540°C (Löw 1987) and 450–550°C (Heinrich 1986). However, they are less than the 640°C proposed for this area by Dale and Holland (2003). This higher temperature estimate may be related to a pre-Alpine relic, since Liati et al. (2009) clearly documented a Variscan-age (340–330 Ma) for some HT eclogites in the northern part of the Adula nappe complex. In any case, the temperatures obtained from the northern part of the Adula nappe complex are associated with Alpine-age upper blueschist- to eclogite-facies conditions at considerably higher temperatures during subduction-related HP/LT metamorphic conditions when compared to the surrounding Fe–Mg carpholite-bearing, blueschist-facies metasediments. The spatial and temporal relationships between this upper blueschist- to eclogite-facies event within the northern Adula nappe and the blueschist-facies event and subsequent Barrow-type overprint in the surrounding metasediments are not yet clear. Structural arguments suggest a late-stage differential N-directed emplacement of the Adula nappe into the surrounding metasediments (Wiederkehr et al. 2008).

We therefore decided not to draw the isotemperature contours across the frontal part of the Adula nappe complex in Figs. 6 and 9.

The higher-grade metasediments in the Aul Unit (Steinmann 1994) of the Misox Zone (Fig. 9) that overlies the Adula nappe are devoid of Fe–Mg carpholite. Chloritoid is commonly associated with garnet (Teutsch 1982), which represents a characteristic blueschist-facies assemblage in metasediments (e.g. Agard et al. 2001; Bucher and Bousquet 2007; Bousquet 2008). In addition, isolated occurrences of eclogites within the Misox Zone (i.e. outcrop "Neu Wahli", possibly part of a mélange located in the Aul Unit; Steinmann 1994) that contain glaucophane, garnet and omphacite (30-50% jadeite component; Oberhänsli 1977; Ring 1992; Santini 1992) clearly document that parts of the Misox Zone also experienced an upper blueschist- to eclogite-facies overprint. This indicates that higher temperatures were associated with the early HP-event in this area (Aul Unit). This too is again in agreement with our estimates of peak-metamorphic temperatures similar to those recorded for the HP-stage in the frontal part of the Adula nappe complex (i.e. 500–525°C, samples 190 and 191). The overall thermal structure of the Misox Zone is characterized by southwards increasing metamorphic conditions, as already reported in several studies ranging from greenschist- to middle amphibolite-facies (e.g. Thompson 1976; Teutsch 1982; Ferreiro Mählmann et al. 2002; Petrova et al. 2002). The strong metamorphic gradient within the Misox Zone was previously documented by Thompson (1976) based on the construction of steeply N-dipping isograds (50–70°), perfectly in line with the closely spaced isotemperature contours in the southern Misox Zone (Fig. 9) revealed by the RSCM method. Staurolite first appears in the southernmost part of the Misox Zone, i.e. south of the 500°C isotemperature contour, and indicates that the southern part of the Misox Zone was affected by lower/middle amphibolite-facies Barrovian overprint (Fig. 9; Wenk 1970; Thompson 1976; Teutsch 1982). Teutsch (1982) determined metamorphic conditions of 0.5–0.7 GPa and 500–550°C near Mesocco, an area where we obtained 530–540°C (samples 185 & 186, Table 1). Note that here in the south the temperatures during late-stage collision-related Barrovian overprint, which led to the growth of staurolite, may not differ significantly from those related to the earlier subduction-related high-pressure event that may have reached eclogite-facies in the southernmost Misox Zone. In any case, the temperatures related to the eclogite-facies event continuously increase southwards, also within the adjacent Adula nappe complex (i.e. Heinrich 1982, 1986). This reflects the southward subduction of tectonic units during the formation of the Alpine orogenic belt. Nagel et al. (2002) demonstrated that near-isothermal decompression led to the growth of staurolite by paragonite breakdown. Hence, within the southernmost Misox Zone, it may become impossible to attribute the RSCM-derived temperatures to either the subduction-related HP-event or the collision-related Barrovian overprint (indicated by stippled P–T-paths in Fig. 9). Here, the Barrow-type overprint either results from isothermal decompression from an eclogitic stage as proposed by Nagel et al. (2002), or alternatively, it may result from a separate heating pulse as proposed by Engi et al. (2001) and Brouwer et al. (2005).

Relationships between isotemperature contours and the polyphase thermal evolution of the metasediments

Wiederkehr et al. (2008) showed that the first deformational event D1 (Safien phase) related to the formation of an accretionary wedge and subduction of the Valais Ocean and parts of the distal European margin is associated with blueschist-facies metamorphism (350–400°C, 1.2–1.4 GPa). This is documented by Fe–Mg carpholite preserved as hair-like fibres in veins consisting of quartz and calcite. Substantial decompression to greenschist-facies conditions was associated with D2 nappe-stacking that led to thrusting of HP-rocks onto LP-units (Ferrera phase). Interestingly, the isotemperature contours in the eastern part of the working area reflect the effect of the D3 (Domleschg phase) nappe-refolding phase, particularly that of the most prominent D3 structure, the Lunschania antiform (Figs. 1, 2; Voll 1976; Kupferschmid 1977; Steinmann 1994; Weh and Froitzheim 2001).

The new RSCM temperature data show that progressive Barrovian overprinting related to the Lepontine thermal dome in the southwestern part of the study area clearly post-dates this D3 event (Wiederkehr et al. 2008); the isotemperature contours crosscut the Lunschania structure at temperatures higher than those reached during the blueschist-facies event and/or subsequent greenschist-facies overprint, i.e. above 450°C (Figs. 6, 8 and 9). The isotemperature contours established for the western part of the study area rather spectacularly crosscut structures, both viewed along strike and within the N–S profile (Fig. 8). This demonstrates the power of the RSCM method for revealing the 3-D geometry of the temperature field during late-stage collision-related metamorphism. Note, however, that the original shape of the isotemperature contours may have been somewhat modified by the last tectonic event (D4, Chièra phase) that is associated with back-folding and the formation of the Northern Steep Belt further to the west (Milnes 1974). This also slightly affected the southwestern part of the study area.

Our study is the first to reveal a jump in maximum temperatures across the contact of the Adula nappe

complex (internal Mesozoic) with the surrounding Valais Ocean-derived metasediments (Figs. 6, 9). Hence, the resolution of the temperature pattern in the northeastern part of the Lepontine dome is much better than in earlier studies (e.g. Todd and Engi 1997). The thermal discontinuity clearly shows that peak-metamorphic temperatures of the northern Adula nappe complex were reached before nappe-stacking, i.e. during the early HP-stage rather than during the late-stage Barrovian overprint. In the southernmost Misox Zone, high temperatures were already reached during the early HP imprint prior to isothermal decompression in this southerly area (e.g. Nagel 2008). Hence, it is impossible to distinguish between the temperatures reached during the two events in the southernmost Misox Zone.

Implications for the tectono-metamorphic evolution and timing constraints

As discussed earlier and summarized in Fig. 9, high-resolution three-dimensional mapping of isotemperature contours in map and profile view faithfully reflects the current distribution of peak-metamorphic temperatures that resulted from the superposition of at least three distinct metamorphic events. This leads to the following observations: (1) Within the northeastern rim of the Lepontine dome—both along and across strike—the isotemperature contours in the 450–570°C range clearly cut across nappe contacts and large-scale, post-nappe folds deforming such contacts; (2) further to the NE, the 350–425°C isotemperature contours are folded by large-scale, post-nappe folds; (3) the substantial jump in maximum temperatures across the tectonic contact between the frontal Adula nappe complex (500–520°C) and the surrounding Valais Ocean-derived metasediments (410–430°C) indicates that this contact accommodated differential tectonic movement of the Adula nappe with respect to the enveloping Bündnerschiefer. This movement must have taken place after the temperature peak was reached within the Adula nappe (sometime between 43 and 35 Ma; see "Discussion" and references in Wiederkehr et al. 2009). The temperatures reached within the enveloping Bündnerschiefer during the late-stage Lepontine event (19–18 Ma; Janots et al. 2008; Wiederkehr et al. 2009) obviously were not as high as those attained during the much earlier high-pressure event within the frontal Adula nappe.

To understand the complex polyphase metamorphic evolution of the study area (see Wiederkehr et al. 2008, 2009 for details), it is essential to relate the peak-metamorphic temperatures presented in this study to specific metamorphic stages, i.e. subduction-related HP-metamorphism or collision-related Barrovian overprint. An unambiguous correlation of peak-metamorphic temperatures is particularly crucial for tectonic units that followed a bimodal P–T-path with an earlier HP/LT event followed by a later thermal overprint. Combined with recent isotopic age constrains presented for the study area (Allaz 2008; Janots et al. 2009; Wiederkehr et al. 2009), we attempt to link the detected RSCM temperatures to the pressure–temperature-time paths of the different tectonic units in order to better understand the temperature distribution map in Fig. 9.

Units characterized by a single loop P–T-path

This group of tectonic units comprises the LP/LT parts of the Grava nappe exposed in the Prättigau half-window, the Scopi Unit and the Urseren-Garvera Zone (Fig. 9). Until now, there has been no reported evidence for an earlier HP/LT metamorphic event in these units. Consequently, all recorded RSCM temperatures represent peak-metamorphic temperatures established along the prograde path of the metamorphic evolution. These range from lower greenschist-facies conditions in the Prättigau half-window to lower/middle amphibolite-facies in the vicinity of Lukmanier. Recent isotopic studies clearly show that lower to middle amphibolite-facies metamorphism in the NE Lepontine dome (western Scopi Unit, Lukmanier; Fig. 9) is young and that peak-metamorphic conditions were reached about 19–18 Ma ago (Allaz 2008; Janots et al. 2009; Wiederkehr et al. 2009). The existence of an earlier and widespread greenschist-facies metamorphic event was pointed out by isotopic studies revealing ages of 32–29 Ma in the Lukmanier area (Janots et al. 2009) and in the Grisons and Engadine window further to the northeast (Wiederkehr et al. 2009). Consequently, the recorded peak-metamorphic temperatures of the eastern Scopi Unit along the Val Lumnezia south of Ilanz (350–400°C) and of the LP/LT units in the Prättigau half-window (150–300°C) are attributed to this Oligocene greenschist-facies overprint. Unfortunately, there are no age constraints for the Urseren-Garvera Zone (375–450°C). However, the work of Janots et al. (2009) indicates that the same 32–29 Ma age range most likely also applies to this greenschist-facies event.

Carpholite-bearing HP/LT units characterized by a bimodal P–T-path

This group comprises the Grava and Tomül nappes derived from the Valais Ocean as well as the Peiden slices and Piz Terri-Lunschania Unit scraped off the adjacent distal European margin, both covering most of the area of investigation between Pizzo Molare in the SW to Chur in the NE (Fig. 9). As discussed earlier, the thermal structure recorded in the northeast is characterized by isotemperature contours that are folded around the Lunschania antiform,

whereas in the southwest the isotemperature contours clearly cut through this antiform. Hence, the thermal structure in the northeast is older than the formation of the Lunschania antiform whereas that in the southwest is younger. The thermal structure characterized by the younger crosscutting isotemperature contours (450–575°C) is clearly related to the lower/middle amphibolite-facies Barrovian overprint of the northeastern Lepontine thermal dome, where peak conditions were established as late as 19–18 Ma ago (Allaz 2008; Janots et al. 2009; Wiederkehr et al. 2009). The temperatures reached during this late metamorphic event were considerably higher than those reached during the earlier HP/LT stage. The thermal structure in the east, on the other hand, is characterized by folded isotemperature contours (350–425°C) and hence reflects conditions established during the earlier HP/LT stage (at around 43–40 Ma for the Valaisan domain; Wiederkehr et al. 2009) and/or during subsequent decompression leading to greenschist-facies overprint. Unfortunately, the peak-metamorphic temperatures are rather similar during both these stages (at 350–400°C) that predate the Barrovian overprint found further west. Hence, a clear separation of maximum temperatures prevailing at peak-pressure conditions from those prevailing during decompression cannot be made. For the following reasons, we favour the interpretation that the folded isotemperature contours in the east reflect a greenschist-facies thermal structure related to the decompression stage: (1) The constructed isotemperature contours can be traced continuously across the boundary between HP and LP-units and therefore clearly post-date syn-D1 HP/LT metamorphism in the Valaisan domain (Wiederkehr et al. 2008); (2) The spacing of the recorded isotemperature contours that reflect the thermal gradient is far too large for blueschist-facies conditions and therefore was probably established during decompression-related greenschist-facies overprinting rather than during blueschist-facies HP/LT metamorphism. Wiederkehr et al. (2009) posited an age of 32–29 Ma for this retrograde greenschist-facies metamorphism that overprints the earlier HP/LT stage and pre-dates the much younger Barrovian overprint found in the W.

Northern Adula nappe complex and Misox Zone

The substantial jump in maximum temperatures across the tectonic contact between the frontal Adula nappe complex (500–525°C) and the surrounding metasediments of the Valaisan (400–450°C; Fig. 9) indicates that the thermal structure preserved inside the Adula nappe complex was established before the final emplacement of the Adula nappe. The estimated peak-metamorphic temperatures are perfectly in line with thermobarometric calculations, reflecting conditions established during subduction-related blueschist/eclogite-facies metamorphism within the Adula nappe (e.g. Heinrich 1986; Löw 1987). Several studies estimate this subduction-related metamorphism to have occurred at about 43–35 Ma ago (Gebauer et al. 1992; Gebauer 1996; Becker 1993; Brouwer et al. 2005; see also reviews given by Berger and Bousquet 2008; Nagel 2008).

A clear attribution of the samples from the Misox Zone that are devoid of Fe–Mg carpholite to a specific metamorphic event is impossible due to the significantly lower sampling density and the complex tectonic evolution of the Misox Zone. Furthermore, the Misox Zone is a narrow, highly tectonized narrow thrust zone (mélange zone), further complicating a clear distinction between a HP/LT stage and subsequent Barrovian overprinting. Only the highest temperatures of 540–550°C measured south of the village of Mesocco, as well as the occurrence of newly grown staurolite nearby, can most probably be attributed to the amphibolite-facies Barrow-type "Lepontine" event. Towards the north, no unambiguous correlation of RSCM-derived temperatures with a specific metamorphic stage or overprint is possible (Fig. 9). The only exceptions to this are samples 190 and 191 (pre-kinematic garnet-chloritoid micaschist) that reveal peak-metamorphic temperatures of 500–525°C and can clearly be attributed to the HP/LT stage (see "Discussion" above).

Discussion of possible reasons leading to inter-sample heterogeneities

There are a small number of samples (i.e. 16 out of a total of 214) that are characterized by abnormally high variation with respect to neighbouring specimens. In general, these samples exhibit much higher peak-metamorphic temperatures compared to those detected in the surrounding locations. These locations are highlighted with bold letters in Table 1 and were not used for the construction of the isotemperature contours presented in Figs. 6, 8 and 9. In the following, we discuss the possible reasons of the detected inter-sample heterogeneities.

In general, samples yielding exceptionally high temperatures can be subdivided into two groups: A first group marked by samples showing a completely different mineral assemblage with respect to the neighbouring locations, and a second group showing no obvious differences in mineral composition. Samples 44, 51, 84, 86, 97, 115, 136, 139, 140 and 210 (Table 1) belong to the second group. Careful analysis of some samples from this second group (specimens 97, 136 and 139 originating form the Piz Terri-Lunschania Unit; Table 1) shows the presence of large and randomly oriented, isolated flakes of white mica, which are clearly of detrital origin. This clearly supports the interpretation that depositional mixing of sedimentary detritus (e.g. Diessel et al. 1978; Itaya 1981; Petrova et al. 2002)

may yield peak temperatures that are valid for the source area rather than for the sampled metasediments. We regard it as likely that depositional mixing of graphite of different degree of graphitization must have occurred in this case and that such mixing is the most likely cause of the scatter among the samples belonging to this group. A study performed along the metamorphic profile from the Prättigau half-window to the Misox Zone provided evidence for the occurrence of detrital graphite in nearly all samples, as is documented by X-ray diffraction data (Petrova et al. 2002). This interpretation is in line with the findings of Galy et al. (2008) that recycling of graphite is responsible for the widespread presence of detrital graphite in natural metamorphic rocks.

The first group comprises samples 190 and 191 (Table 1) that originate from the Misox Zone, and hence, from an area close to the contact with the Adula nappe complex; specimens 146, 147, 148 and 149 are from within the Adula nappe complex. As clearly indicated in Table 1, these samples are characterized by mineral assemblages that are different from those found in the neighbouring metasedimentary samples. This points to a relatively higher grade of metamorphism within the Adula nappe and parts of the immediately adjacent Misox Zone. Hence, the inter-sample heterogeneities detected in this group of samples definitely do not stem from a methodological artefact, but they simply reflect different peak-metamorphic conditions within different tectonic units that are offset by later motion of the Adula nappe and parts of the Misox Zone with respect to the surrounding metasediments. We consider the 500–525°C temperatures recorded by these specimens to be related to an upper blueschist- to eclogite-facies event that had considerably higher temperatures than the surrounding Fe–Mg carpholite-bearing blueschist-facies rocks, and that only affected the Adula nappe complex and immediately adjacent parts of the Misox Zone. These temperatures are consistent with earlier thermobarometric calculations (Heinrich 1986; Löw 1987).

Conclusions

Raman spectroscopy of a large sampling of carbonaceous material from metasediments at the margin of the Lepontine dome allows for a comparison of the Beyssac et al. (2002a) and Rahl et al. (2005) calibrations in the 150–600°C temperature range. The two calibration methods yield essentially identical inferred maximum temperatures above 330°C, with discrepancies of less than 30°C. At lower temperatures, only the Rahl et al. (2005) calibration yields a reliable maximum temperature field gradient. The method can be applied successfully to specimens of low-grade metasediments (so-called Bündnerschiefer) that are devoid of diagnostic mineral assemblages and are therefore unsuited for accurate estimation of the metamorphic temperature based on equilibrium thermodynamics of coexisting mineral phases.

The results of the three-dimensional mapping of isotemperature contours show that the maximum temperature field gradients inferred from Raman spectroscopy of carbonaceous material faithfully reflect the current distribution of peak-metamorphic temperatures resulting from the superposition of distinct metamorphic events. This conclusion is corroborated by independent petrological and structural data (e.g. Wiederkehr et al. 2008). It was found that the maximum temperatures obtained with the RSCM method compare favourably with temperatures inferred from other petrological data, e.g. from P–T calculations and distribution of diagnostic mineral assemblages (e.g. Chadwick 1968; Frey 1969; Fox 1975; Heinrich 1986; Löw 1987; Engi et al. 1995; Todd and Engi 1997; Bousquet et al. 2002; Rahn et al. 2002; Wiederkehr 2009). The temperatures reflect the maximum temperatures reached, also in areas that underwent a polyphase thermal evolution. The three-dimensional character of those parts of the constructed contours that reflect the same metamorphic event yield useful information on the relationship between deformation and metamorphism. Finally, our data support the assumption that the transformation of CM to graphite is a continuous and a mainly temperature-dependent process.

Nevertheless, some samples are characterized by a large scatter of estimated mean temperature, whereas others predict peak-metamorphic temperatures that vary among neighbouring samples. Dealing with such discrepancies that come from naturally heterogeneous carbonaceous matter is a common challenge when using the RSCM method (e.g. Beyssac et al. 2002b, 2003; compare also first section of paragraph "Mapping thermal field gradients in 3 dimensions"). In this study, depositional mixing of sedimentary detritus originating from different metamorphic sources (e.g. Diessel et al. 1978; Itaya 1981; Petrova et al. 2002) is one important factor.

The investigation of CM by Raman spectroscopy revealed at least three different thermal regimes as inferred from overprinting criteria between the constructed isotemperature contours and observed structures: (1) Within the northeastern rim of the Lepontine dome the isotemperature contours associated with the collision-related, late-stage Barrow-type event clearly cut across nappe contacts and post-nappe folds, both along and across strike; (2) Further to the northeast, the isotemperature contours reflect temperatures reached during an earlier blueschist-facies event and/or during subsequent near-isothermal decompression and are folded around large-scale post-nappe-stacking folds; (3) A substantial jump in maximum temperatures across the tectonic contact between the

frontal Adula nappe complex and surrounding Valais Ocean-derived metasediments indicates that this contact accommodated differential tectonic movement of the Adula nappe with respect to the enveloping Bündnerschiefer. This must have occurred after the attainment of maximum temperatures within the northern Adula nappe.

When combined with recent isotopic ages, the RSCM temperatures in our study provide important information for reconstructing the polyphase metamorphic evolution of the Central Alps, from subduction-related HP/LT metamorphism to collision-related, Barrow-type thermal overprinting.

Acknowledgments Excellent preparation of numerous samples by W. Tschudin, as well as great support in the field by G. Derungs, both members of Basel University, are gratefully acknowledged. The use of the samples from the study by Petrova et al. (2002) as well as from the collection of M. Frey (Basel University) is acknowledged. A. Riemann from Potsdam University is thanked for a supportive field trip as well as for the help in the Raman laboratory of Potsdam University. O. Beyssac and R. Ferreiro Mählmann are thanked for their comments and suggestions that improved the quality of an earlier version this manuscript. The paper benefited from the careful and constructive reviews of M. Engi and an anonymous reviewer. The helpful editorial comments of M. Handy substantially improved the quality of the manuscript. Funding by the Swiss National Science Foundation (project NF-200020-113585 and precursor project NF-200020-103585) is gratefully acknowledged. S.M. Schmid acknowledges support by the Alexander-von-Humboldt Foundation during the final stages of the synthesis of the data presented here.

References

Agard P, Jolivet L, Goffé B (2001) Tectonometamorphic evolution of the Schistes Lustrés complex: implications for the exhumation of HP and UHP rocks in the Western Alps. Bull Soc Geol Fr 172:617–636

Allaz J (2008) Metamorphic evolution in the northern Central Alps: linking ^{39}Ar-^{40}Ar dating with thermobarometry. Unpublished PhD thesis, Universität Bern

Angiboust S, Agard P, Jolivet L, Beyssac O (2009) The Zermatt-Saas ophiolite: the largest (60-km wide) and deepest (c. 70–80 km) continuous slice of oceanic lithosphere detached from a subduction zone? Terra Nova 21:171–180

Aoya M, Kouketsu Y, Endo S, Shimizu, H, Mizukami T, Nakamura D, Wallis S (2010) Extending the applicability of the Raman carbonaceous-material geothermometer using data from contact metamorphic rocks. J Metamorph Geol. doi:10.1111/j.1525-1314.2010.00896.x

Baumer A, Frey JD, Jung W, Uhr A (1961) Die Sedimentbedeckung des Gotthard-Massivs zwischen oberen Bleniotal und Lugnez (Vorläufige Mitteilung). Eclogae Geol Helv 54:478–491

Becker H (1993) Garnet peridotite and eclogite Sm-Nd mineral ages from the Lepontine dome (Swiss Alps)—new evidence for Eocene high-pressure metamorphism in the Central Alps. Geology 21:599–602

Berger A, Bousquet R (2008) Subduction-related metamorphism in the Alps: Review of isotopic ages based on petrology and their geodynamic consequences. In: Siegesmund S et al. (eds) Tectonic aspects of the Alpine-Dinaride-Carpathian system. Geological Society of Special Publications, vol 298, pp 117–144

Berger A, Mercolli I, Engi M (2005) The central Lepontine Alps: notes accompanying the tectonic and petrographic map sheet Sopra Ceneri (1:100'000). Schweiz Mineral Petrogr Mitt 85:109–146

Berger A, Rosenberg C, Schaltegger U (2009) Stability and isotopic dating of monazite and allanite in partially molten rocks: example from the Central Alps. Swiss J Geosci 102:15–29

Beyssac O, Goffé B, Chopin C, Rouzaud JN (2002a) Raman spectra of carbonaceous material in metasediments: a new geothermometer. J Metamorph Geol 20:859–871

Beyssac O, Rouzaud JN, Goffé B, Brunet F, Chopin C (2002b) Graphitization in a high-pressure, low-temperature metamorphic gradient: a Raman microspectroscopy and HRTEM study. Contrib Mineral Petrol 143:19–31

Beyssac O, Brunet F, Petitet JP, Goffé B, Rouzaud JN (2003a) Experimental study of the microtextural and structural transformations of carbonaceous materials under pressure and temperature. Eur J Mineral 15:937–951

Beyssac O, Goffé B, Petitet JP, Froigneux E, Moreau M, Rouzaud JN (2003b) On the characterization of disordered and heterogeneous carbonaceous materials by Raman spectroscopy. Spectrochim Acta Part A Mol Biomol Spectrosc 59:2267–2276

Beyssac O, Bollinger L, Avouac JP, Goffé B (2004) Thermal metamorphism in the lesser Himalaya of Nepal determined from Raman spectroscopy of carbonaceous material. Earth Planet Sci Lett 225:233–241

Beyssac O, Simoes M, Avouac JP, Farley KA, Chen YG, Chan YC, Goffé B (2007) Late Cenozoic metamorphic evolution and exhumation of Taiwan. Tectonics 26:TC6001. doi:10.1029/2006tc002064

Bollinger L, Avouac JP, Beyssac O, Catlos EJ, Harrison TM, Grove M, Goffé B, Sapkota S (2004) Thermal structure and exhumation history of the Lesser Himalaya in central Nepal. Tectonics 23:TC5015. doi:10.1029/2003tc001564

Bonijoly M, Oberlin M, Oberlin A (1982) A possible mechanism for natural graphite formation. Int J Coal Geol 1:238–312

Bousquet R (2008) Metamorphic heterogeneities within a single HP unit: overprint effect or metamorphic mix? Lithos 103:46–69

Bousquet R, Goffé B, Henry P, Le Pichon X, Chopin C (1997) Kinematic, thermal and petrological model of the central alps: Lepontine metamorphism in the upper crust and eclogitisation of the lower crust. Tectonophysics 273:105–127

Bousquet R, Oberhänsli R, Goffé B, Jolivet L, Vidal O (1998) High-pressure-low-temperature metamorphism and deformation in the Bündnerschiefer of the Engadine window: implications for the regional evolution of the eastern Central Alps. J Metamorph Geol 16:657–674

Bousquet R, Goffé B, Vidal O, Oberhänsli R, Patriat M (2002) The tectono-metamorphic history of the Valaisan domain from the Western to the Central Alps: new constraints on the evolution of the Alps. Geol Soc Am Bull 114:207–225

Bousquet R, Oberhänsli R, Goffé B, Wiederkehr M, Koller F, Schmid SM, Schuster R, Engi M, Berger A, Martinotti G (2008) Metamorphism of metasediments in the scale of an orogen: A key to the Tertiary geodynamic evolution of the Alps. In: Siegesmund S et al. (eds) Tectonic aspects of the Alpine-Dinaride-Carpathian system. Geological Society of Special Publications, vol 298, pp 393–411

Brouwer FM, Burri T, Engi M, Berger A (2005) Eclogite relics in the Central Alps: PT-evolution, Lu-Hf ages, and implications for formation of tectonic mélange zones. Schweiz Mineral Petrogr Mitt 85:147–174

Bucher S, Bousquet R (2007) Metamorphic evolution of the Briançonnais units along the ECORS-CROP profile (Western Alps): new data on metasedimentary rocks. Swiss J Geosci 100:227–242

Buseck PR, Huang B-J (1985) Conversion of carbonaceous material to graphite during metamorphism. Geochim Cosmochim Acta 49:2003–2016

Bustin RM, Ross JV, Moffat I (1986) Vitrinite anisotropy under differential stress and high confining pressure and temperature: preliminary observations. Int J Coal Geol 6:343–351

Bustin RM, Ross JV, Rouzaud JN (1995) Mechanisms of graphite formation from kerogen: experimental evidence. Int J Coal Geol 28:1–36

Cançado LG, Takai K, Enoki T, Endo M, Kim YA, Mizusaki H, Jorio A, Coelho LN, Magalhaes-Paniago R, Pimenta MA (2006) General equation for the determination of the crystallite size L_a of nanographite by Raman spectroscopy. Appl Phys Lett 88:163106

Cançado LG, Jorio A, Pimenta MA (2007) Measuring the absolute Raman cross section of nanographites as a function of laser energy and crystallite size. Phys Rev B 76:064304

Chadwick B (1968) Deformation and Metamorphism in the Lukmanier Region, Central Switzerland. Geol Soc Am Bull 79: 1123–1150

Dale J, Holland TJB (2003) Geothermobarometry, P-T paths and metamorphic field gradients of high-pressure rocks from the Adula Nappe, Central Alps. J Metamorph Geol 21:813–830

Derungs G (2008) Structural and metamorphic evolution of metasediments at the contact between Valaisan Oceanic domain and adjacent distal European margin. Unpublished Master thesis, Universität Basel

Diessel CFK, Brothers RN, Black PM (1978) Coalification and graphitization in high-pressure schists in New Caledonia. Contrib Mineral Petrol 68:63–78

Engi M, Todd CS, Schmatz DR (1995) Tertiary metamorphic conditions in the eastern Lepontine Alps. Schweiz Mineral Petrogr Mitt 75:347–369

Engi M, Berger A, Roselle GT (2001) Role of the tectonic accretion channel in collisional orogeny. Geology 29:1143–1146

Engi M, Bousquet R, Berger A (2004) Explanatory notes to the map: metamorphic structure of the Central Alps. Mitt Österr Geol Ges 149:157–173

Etter U (1987) Stratigraphische und strukturgeologische Untersuchungen im gotthardmassivischen Mesozoikum zwischen dem Lukmanierpass und der Gegend von Ilanz. Unpublished PhD thesis, Universität Bern

Ferreiro Mählmann R, Petrova TV, Pironon J, Stern WB, Ghanbaja J, Dubessy J, Frey M (2002) Transmission electron microscopy study of carbonaceous material in a metamorphic profile from diagenesis to amphibolite facies (Bündnerschiefer, Eastern Switzerland). Schweiz Mineral Petrogr Mitt 82:253–272

Fox JS (1975) Three-dimensional isograds from the Lukmanier-Pass, Switzerland, and their tectonic significance. Geol Mag 112: 547–564

French BM (1964) Graphitization of organic material in a progressively metamorphosed Precambrian iron formation. Science 146:917–918

Frey M (1969) Die Metamorphose des Keupers vom Tafeljura bis zum Lukmanier-Gebiet. Beitr Geol Kt Schweiz NF 137:1–160

Frey M (1974) Alpine metamorphism of pelitic and marly rocks of the Central Alps. Schweiz Mineral Petrogr Mitt 54:489–506

Frey M (1978) Progressive low-grade metamorphism of a black shale formation, Central Swiss Alps, with special reference to Pyrophyllite and Margarite bearing assemblages. J Petrol 19: 95–135

Frey M, Ferreiro Mählmann R (1999) Alpine metamorphism of the central Alps. Schweiz Mineral Petrogr Mitt 79:135–154

Frey M, Bucher K, Frank E, Mullis J (1980) Alpine metamorphism along the geotraverse Basel-Chiasso—a review. Eclogae Geol Helv 73:527–546

Frey M, Bucher K, Frank E, Schwander H (1982) Margarite in the Central Alps. Schweiz Mineral Petrogr Mitt 62:21–45

Frey M, Desmons J, Neubauer F (1999) Metamorphic map of the Alps. 1:500'000. Schweiz Mineral Petrogr Mitt 79

Frisch W (1979) Tectonic progradation and plate tectonic evolution of the Alps. Tectonophysics 60:121–139

Froitzheim N, Schmid SM, Conti P (1994) Repeated change from crustal shortening to orogen-parallel extension in the Austroalpine units of Graubünden. Eclogae Geol Helv 87:559–612

Froitzheim N, Schmid SM, Frey M (1996) Mesozoic paleogeography and the timing of eclogite-facies metamorphism in the Alps: a working hypothesis. Eclogae Geol Helv 89:81–110

Gabalda S, Beyssac O, Jolivet L, Agard P, Chopin C (2009) Thermal structure of a fossil subduction wedge in the Western Alps. Terra Nova 21:28–34

Galy V, Beyssac O, France-Lanord C, Eglinton T (2008) Recycling of graphite during Himalayan erosion: a geological stabilization of carbon in the crust. Science 322:943–945

Gansser A (1937) Der Nordrand der Tambodecke. Schweiz Mineral Petrogr Mitt 17:291–523

Gebauer D (1996) A P-T-t path for a high-pressure ultramafic rock-association and their felsic country-rocks based on SHRIMP-dating of magmatic and metamorphic zircon domains. Example: Alpe Arami (Central Swiss Alps). In: Hart A, Basu SR (eds) Reading the isotope code. American Geophysical Union, Washington D.C., pp 307–328

Gebauer D, Grünenfelder M, Tilton G, Trommsdorff V, Schmid SM (1992) The geodynamic evolution of garnet-peridotites, garnet-pyroxenites and eclogites of Alp Arami and Cima di Gagnone (Central Alps) from Early Proterozoic to Oligocene. Schweiz Mineral Petrogr Mitt 72:107–111

Goffé B, Bousquet R (1997) Ferrocarpholite, chloritoïde et lawsonite dans les métapelites des unités du Versoyen et du Petit St. Bernard (zone valaisanne, Alpes occidentales). Schweiz Mineral Petrogr Mitt 77:137–147

Goffé B, Chopin C (1986) High-pressure metamorphism in the Western Alps: zoneography of metapelites, chronology and consequences. Schweiz Mineral Petrogr Mitt 66:41–52

Goffé B, Oberhänsli R (1992) Ferro- and magnesiocarpholite in the "Bündnerschiefer" of the eastern Central Alps (Grisons and Engadine Window). Eur J Mineral 4:835–838

Goffé B, Bousquet R, Henry P, Le Pichon X (2003) Effect of the chemical composition of the crust on the metamorphic evolution of orogenic wedges. J Metamorph Geol 21:123–141

Grew ES (1974) Carbonaceous material in some metamorphic rocks of New England and other areas. J Geol 82:50–73

Guedes A, Noronha F, Prieto AC (2005) Characterisation of dispersed organic matter from lower Palaeozoic metasedimentary rocks by organic petrography, X-ray diffraction and micro-Raman spectroscopy analyses. Int J Coal Geol 62:237–249

Handy MR, Oberhänsli R (2004) Age map of the metamorphic structure of the Alps—tectonic interpretation and outstanding problems. Mitt Österr Geol Ges 149:201–226

Handy MR, Schmid SM, Bousquet R, Kissling E, Bernoulli D (2010) Reconciling plate-tectonic reconstructions of Alpine Tethys with the geological-geophysical record of spreading and subduction in the Alps. Earth Sci Rev 102:121–158

Heinrich CA (1982) Kyanite-eclogite to amphibolite facies evolution of hydrous mafic and pelitic rocks, Adula-nappe, Central Alps. Contrib Mineral Petrol 81:30–38

Heinrich CA (1986) Eclogite facies regional metamorphism of hydrous mafic rock in the Central Alpine Adula Nappe. J Petrol 27:123–154

Hoefs J, Frey M (1976) The isotopic composition of carbonaceous matter in a metamorphic profile from the Swiss Alps. Geochim Cosmochim Acta 40:945–951

Hunziker JC, Desmons J, Hurford AJ (1992) Thirty-two years of geochronological work in the Central and Western Alps: a review on seven maps. Mem Geol Univ Lausanne

Itaya T (1981) Carbonaceous material in pelitic schists of the Sanbagawa metamorphic belt in central Shikoku, Japan. Lithos 14:215–224

Janots E, Engi M, Berger A, Allaz J, Schwarz JO, Spandler C (2008) Prograde metamorphic sequence of REE minerals in pelitic rocks of the Central Alps: implications for allanite-monazite-xenotime phase relations from 250 to 610°C. J Metamorph Geol 26:509–526

Janots E, Engi M, Rubatto D, Berger A, Gregory C, Rahn MK (2009) Metamorphic rates in collisional orogeny from in situ allanite and monazite dating. Geology 37:11–14

Jenny H, Frischknecht G, Kopp J (1923) Geologie der Adula. Beitr Geol Kt Schweiz NF 51:1–123

Judik K, Rantitsch G, Rainer TM, Arkai P, Tomljenovic B (2008) Alpine metamorphism of organic matter in metasedimentary rocks from Mt. Medvednica (Croatia). Swiss J Geosci 101: 605–616

Köppel V, Günthert A, Grünenfelder M (1981) Patterns of U-Pb zircon and monazite ages in polymetamorphic units of the Swiss Alps. Schweiz Mineral Petrogr Mitt 61:97–119

Kribek B, Hrabal J, Landais P, Hladikova J (1994) The association of poorly ordered graphite, coke and bitumens in greenschist facies rocks of the Ponikla Group, Lugicum, Czech Republic: the result of graphitization of various types of carbonaceous matter. J Metamorph Geol 12:493–503

Kribek B, Sykorova I, Machovic V, Laufek F (2008) Graphitization of organic matter and fluid-deposited graphite in Palaeoproterozoic (Birmian) black shales of the Kaya-Goren greenstone belt (Burkina Faso, West Africa). J Metamorph Geol 26:937–958

Kupferschmid C (1977) Geologie auf der Lugnezer Seite der Piz Aul-Gruppe. Eclogae Geol Helv 70:1–58

Lahfid A, Beyssac O, Deville E, Negro F, Chopin C, Goffe B (2010) Evolution of the Raman spectrum of carbonaceous material in low-grade metasediments of the Glarus Alps (Switzerland). Terra Nova 22:354–360

Landis CA (1971) Graphitization of dispersed carbonaceous material in metamorphic rocks. Contrib Mineral Petrol 30:34–45

Large DJ, Christy AG, Fallick AE (1994) Poorly crystalline carbonaceous matter in high grade metasediments: implications for graphitisation and metamorphic fluid composition. Contrib Mineral Petrol 116:108–116

Lee YJ (2004) The second order Raman spectroscopy in carbon crystallinity. J Nucl Mater 325:174–179

Liati A, Gebauer D, Fanning CM (2009) Geochronological evolution of HP metamorphic rocks of the Adula nappe, Central Alps, in pre-Alpine and Alpine subduction cycles. J Geol Soc 166:797–810. doi:10.1144/0016-76492008-033

Livi KJT, Ferry JM, Veblen DR, Frey M, Connolly JAD (2002) Reactions and physical conditions during metamorphism of Liassic aluminous black shales and marls in central Switzerland. Eur J Mineral 14:647–672

Loprieno A, Bousquet R, Bucher S, Ceriani S, Dalla Torre FH, Fügenschuh B, Schmid SM (2010) The Valais units in Savoy (France): a key area for understanding the paleogeography and the tectonic evolution of the Western Alps. Int J Earth Sci (this volume). doi:10.1007/s00531-010-0595-1

Löw S (1987) Die tektono-metamorphe Entwicklung der nördlichen Adula-Decke. Beitr Geol Kt Schweiz NF 161:1–84

Matthews MJ, Pimenta MA, Dresselhaus G, Dresselhaus MS, Endo M (1999) Origin of dispersive effects of the Raman D band in carbon materials. Phys Rev B 59:6585–6588

Milnes AG (1974) Structure of Pennine zone (Central Alps)—new working hypothesis. Geol Soc Am Bull 85:1727–1732

Nabholz WK (1945) Geologie der Bündnerschiefergebirge zwischen Rheinwald, Valser- und Safiental. Eclogae Geol Helv 38:1–119

Nagel T (2008) Tertiary subduction, collision, and exhumation recorded in the Adula nappe, central Alps. In: Siegesmund S et al. (eds) Tectonic Aspects of the Alpine-Dinaride-Carpathian system. Geological Society of Special Publications, vol 298, pp 365–392

Nagel T, de Capitani C, Frey M (2002) Isograds and P-T evolution in the eastern Lepontine Alps (Graubünden, Switzerland). J Metamorph Geol 20:309–324

Nänny P (1948) Zur Geologie der Prättigauschiefer zwischen Rhätikon und Plessur. PhD thesis, Universität Zürich

Nasdala L, Smith DC, Kaindl R, Ziemann MA (2004) Raman spectroscopy: analytical perspectives in mineralogical research. In: Beran A, Libowitzky E (eds) Spectroscopic methods in mineralogy. EMU Notes in Mineralogy 6. European Mineralogical Union, Eötvös University Press, Budapest, pp 281–343

Negro F, Beyssac O, Goffé B, Saddiqi O, Bouybaouène ML (2006) Thermal structure of the Alboran Domain in the Rif (northern Morocco) and the Western Betics (southern Spain). Constraints from Raman spectroscopy of carbonaceous material. J Metamorph Geol 24:309–327

Nemanich RJ, Solin SA (1979) First- and second-order Raman scattering from finite-size crystals of graphite. Phys Rev B 20:392–401

Niggli E (1970) Alpine Metamorphose und alpine Gebirgsbildung. Fortschr Mineral 47:16–26

Niggli E, Niggli C (1965) Karten der Verbreitung einiger Mineralien der alpidischen Metamorphose in den Schweizer Alpen (Stilpnomelan, Alkali-Amphibol, Chloritoid, Staurolith, Disthen, Sillimanit). Eclogae Geol Helv 58:335–368

Nover G, Stoll JB, von der Gönna J (2005) Promotion of graphite formation by tectonic stress—a laboratory experiment. Geophys J Int 160:1059–1067

Oberhänsli R (1977) Natriumamphibol-führende metamorphe basische Gesteine aus den Bündnerschiefern Graubündens. Unpublished PhD thesis, ETH Zürich

Oberhänsli R (1978) Chemische Untersuchungen an Glaukophan-führenden basischen Gesteinen aus den Bündnerschiefern Graubündens. Schweiz Mineral Petrogr Mitt 58:139–156

Oberhänsli R (1994) Subducted and obducted ophiolites of the Central Alps: paleotectonic implications deduced by their distribution and metamorphic overprint. Lithos 33:109–118

Oberhänsli R, Goffé B, Bousquet R (1995) Record of a HP-LT metamorphic evolution in the Valais zone: Geodynamic implications. In: Lombardo B (ed) Studies on metamorphic rocks and minerals of the western Alps. A volume in memory of Ugo Pognante. Boll Mus Reg Sci Nat, Torino, vol 13, pp 221–239

Oberhänsli R, Bousquet R, Goffé B (2003) Comment to "Chloritoid composition and formation in the eastern Central Alps: a comparison between Penninic and Helvetic occurrences" by M. Rahn, M. Steinmann & M. Frey. Schweiz Mineral Petrogr Mitt 83:341–344

Oberhänsli R, Bousquet R, Engi M, Goffé B, Gosso G, Handy M, Höck V, Koller F, Lardeaux J-M, Polino R, Rossi P, Schuster R, Schwartz S, Spalla MI (2004) Metamorphic structure of the Alps, 1:1'000'000. In: Oberhänsli R (ed) Explanatory note to the map "Metamorphic structure of the Alps", Commission for the Geological Map of the World, Paris. Mitt Österr Geol Ges 149

Okuyama-Kusunose Y, Itaya T (1987) Metamorphism of carbonaceous material in the Tono conatct aureole, Kitakami Mountains, Japan. J Metamorph Geol 5:121–139

Pasteris JD (1989) In situ analysis in geological thin-sections by Laser Raman microprobe microspectroscopy: a cautionary note. Appl Spectrosc 43:567–570

Pasteris JD, Wopenka B (1991) Raman-spectra of graphite as indicators of degree of metamorphism. Can Mineral 29:1–9

Petrova TV, Ferreiro Mählmann R, Stern WB, Frey M (2002) Application of combustion and DTA-TGA analysis to the study of metamorphic organic matter. Schweiz Mineral Petrogr Mitt 82:33–53

Pimenta MA, Dresselhaus G, Dresselhaus MS, Cançado LG, Jorio A, Saito R (2007) Studying disorder in graphite-based systems by Raman spectroscopy. Phys Chem Chem Phys 9:1276–1291

Pocsik I, Hundhausen M, Koos M, Ley L (1998) Origin of the D peak in the Raman spectrum of microcrystalline graphite. J Non Crystal Solids 227:1083–1086

Probst P (1980) Die Bündnerschiefer des nördlichen Penninikums zwischen Valser Tal und Passo di San Giacomo. Beitr Geol Kt Schweiz NF 153:1–64

Quinn AW, Glass HD (1958) Rank of coal and metamorphic grade of rocks of Narragansett basin of Rhode Island. Econ Geol 53:563–576

Rahl JM, Anderson KM, Brandon MT, Fassoulas C (2005) Raman spectroscopic carbonaceous material thermometry of low-grade metamorphic rocks: Calibration and application to tectonic exhumation in Crete, Greece. Earth Planet Sci Lett 240:339–354

Rahn MK, Steinmann M, Frey M (2002) Chloritoid composition and formation in the eastern Central Alps: a comparison between Penninic and Helvetic occurrences. Schweiz Mineral Petrogr Mitt 82:409–426

Rantitsch G, Judik K (2009) Alpine metamorphism in the central segment of the Western Greywacke Zone (Eastern Alps). Geol Carp 60:319–329

Rantitsch G, Grogger W, Teichert C, Ebner F, Hofer C, Maurer EM, Schaffer B, Toth M (2004) Conversion of carbonaceous material to graphite within the Greywacke Zone of the Eastern Alps. Int J Earth Sci (Geol Rundsch) 93:959–973

Rantitsch G, Sachsenhofer RF, Hasenhüttl C, Russegger B, Rainer T (2005) Thermal evolution of an extensional detachment as constrained by organic metamorphic data and thermal modeling: Graz Paleozoic Nappe Complex (Eastern Alps). Tectonophysics 411:57–72

Ring U (1992) The Alpine geodynamic evolution of Penninic nappes in the eastern Central Alps: geothermobarometric and kinematic data. J Metamorph Geol 10:33–53

Rubatto D, Hermann J, Berger A, Engi M (2009) Protracted fluid-induced melting during Barrovian metamorphism in the Central Alps. Contrib Mineral Petrol 158:703–722

Santini L (1992) Geochemistry and geochronology of the basic rocks of the Penninic nappes of East-Central Alps (Switzerland). Unpublished PhD thesis, Université de Lausanne

Schmid SM, Pfiffner OA, Froitzheim N, Schönborn G, Kissling E (1996) Geophysical-geological transect and tectonic evolution of the Swiss-Italian Alps. Tectonics 15:1036–1064

Schmid SM, Fügenschuh B, Kissling E, Schuster R (2004) Tectonic map and overall architecture of the Alpine orogen. Eclogae Geol Helv 97:93–117

Schmid SM, Bernoulli D, Fügenschuh B, Matenco L, Schefer S, Schuster R, Tischler M, Ustaszewski K (2008) The Alpine-Carpathian-Dinaridic orogenic system: correlation and evolution of tectonic units. Swiss J Geosci 101:139–183

Steinmann MC (1994) Die nordpenninischen Bündnerschiefer der Zentralalpen Graubündens: Tektonik, Stratigraphie und Beckenentwicklung. Unpublished PhD thesis, ETH Zürich

Steinmann M, Stille P (1999) Geochemical evidence for the nature of the crust beneath the eastern North Penninic basin of the Mesozoic Tethys ocean. Geol Rundsch 87:633–643

Streckeisen A, Wenk E (1974) On steep isogradic surfaces in the Simplon area. Contrib Mineral Petrol 47:81–95

Strohbach HE (1965) Der mittlere Abschnitt der Tambodecke samt seiner mesozoischen Unterlage und Bedeutung. Mitt Geol Inst Eidgenöss Tech Hochsch Univ Zürich 38:1–171

Suchy V, Frey M, Wolf M (1997) Vitrinite reflectance and shear-induced graphitization in orogenic belts: a case study from the Kandersteg area, Helvetic Alps, Switzerland. Int J Coal Geol 34:1–20

Tan PH, Dimovski S, Gogotsi Y (2004) Raman scattering of non-planar graphite: arched edges, polyhedral crystals, whiskers and cones. Philos Trans R Soc Lond A 362:2289–2310

Teichmüller M (1987) Organic material and very low-grade metamorphism. In: Frey M (ed) Low-temperature metamorphism. Blacky, Glasgow, pp 114–161

Teutsch R (1982) Alpine Metamorphose der Misoxer-Zone (Bündnerschiefer, Metabasite und granitische Gneise). Unpublished PhD thesis, Universität Bern

Thakur VC (1971) The structural and metamorphic history of the Mesozoic and pre-Mesozoic basement rocks of the Molare region, Ticino, Switzerland. Unpublished PhD thesis, Imperial college of London

Thakur VC (1973) Events in the Alpine deformation and metamorphism in the northern Pennine zone and southern Gotthard massif regions, Switzerland. Geol Rundsch 62:549–563

Thoenen A (1989) A comparative study of garnet-biotite geothermometers. Unpublished PhD thesis, Universität Basel

Thompson PH (1976) Isograd patterns and pressure-temperature distributions during regional metamorphism. Contrib Mineral Petrol 57:277–295

Thüring M (1990) Geologie um den Hennensädel im hinteren Valsertal (GR). Unpublished Diploma thesis, Universität Basel

Todd CS, Engi M (1997) Metamorphic field gradients in the Central Alps. J Metamorph Geol 15:513–530

Tricart P (1984) From passive margin to continental collision: a tectonic scenario for the Western Alps. Am J Sci 284:97–120

Trommsdorff V (1966) Progressive Metamorphose kieseliger Karbonatgesteine in den Zentralalpen zwischen Bernina und Simplon. Schweiz Mineral Petrogr Mitt 46:431–460

Trümpy R (1960) Paleotectonic evolution of the Central and Western Alps. Geol Soc Am Bull 71:843–908

Tuinstra F, Koenig JL (1970) Raman spectrum of graphite. J Chem Phys 53:1126–1130

Van der Plaas L, Hügi T, Mladeck MH, Niggli E (1958) Chloritoid vom Hennensädel südlich Vals (nördliche Aduladecke). Schweiz Mineral Petrogr Mitt 38:237–246

Voll G (1976) Structural Studies of the Valser Rhine Valley and the Lukmanier Region and their Importance for the nappe Structure of the Central Swiss Alps. Schweiz Mineral Petrogr Mitt 56:619–626

Wada H, Tomita T, Matsuura K, Iuchi K, Ito M, Morikiyo T (1994) Graphitization of carbonaceous matter during metamorphism with references to carbonate and pelitic rocks of contact and regional metamorphisms, Japan. Contrib Mineral Petrol 118:217–228

Wang A, Dhamelincourt P, Dubessy J, Guerard D, Landais P, Lelaurain M (1989) Characterization of graphite alteration in an uranium deposit by micro-Raman spectroscopy, X-RAY diffraction, Transmission Electron Microscopy and Scanning Electron Microscopy. Carbon 27:209–218

Weh M (1998) Tektonische Entwicklung der penninischen Sediment-Decken in Graubünden (Prättigau bis Oberhalbstein). Unpublished PhD thesis, Universität Basel

Weh M, Froitzheim N (2001) Penninic cover nappes in the Prattigau half-window (Eastern Switzerland): Structure and tectonic evolution. Eclogae Geol Helv 94:237–252

Wenk E (1962) Plagioklas als Indexmineral in den Zentralalpen. Schweiz Mineral Petrogr Mitt 42:139–152

Wenk E (1970) Zur Regionalmetamorphose und Ultrametamorphose im Lepontin. Fortschr Mineral 47:34–51

Wiederkehr M (2009) From subduction to collision: a combined metamorphic, structural and geochronological study of poly-metamorphic metasediments at the NE edge of the Lepontine dome (Swss Central Alps). Unpublished PhD thesis, Universität Basel

Wiederkehr M, Bousquet R, Schmid SM, Berger A (2008) From subduction to collision: Thermal overprint of HP/LT meta-sediments in the northeastern Lepontine Dome (Swiss Alps) and consequences regarding the tectono-metamorphic evolution of the Alpine orogenic wedge. In: Froitzheim N, Schmid SM (eds) Orogenic processes in the Alpine collision zone. Swiss J Geosci 101(Suppl):S127–S155

Wiederkehr M, Sudo M, Bousquet R, Berger A, Schmid SM (2009) Alpine orogenic evolution from subduction to collisional thermal overprint: the 40Ar/39Ar age constraints from the Valaisan Ocean, Central Alps. Tectonics 28:TC6009. doi:10.1029/2009TC002496

Wopenka B, Pasteris JD (1993) Structural characterization of kerogens to granulite-facies graphite—applicability of Raman microprobe spectroscopy. Am Mineral 78:533–557

Wyss R, Isler A (2007) Blatt 1234 Vals—Geol Atlas Schweiz 1:25'000. Erläut 121:1–78

Yui TF, Huang E, Xu J (1996) Raman spectrum of carbonaceous material: a possible metamorphic grade indicator for low-grade metamorphic rocks. J Metamorph Geol 14:115–124

Ziegler W (1956) Geologische Studien in den Flyschgebieten des Oberhalbsteins (Graubünden). Eclogae Geol Helv 49:1–78

Zulbati F (2008) Structural and metamorphic evolution of the phengite-bearing schists of the northern Adula Nappe (Central Alps, Switzerland). Geol J 43:33–57